SCIENCE CHINA
Earth Sciences

•ARTICLE•

October 2024 Vol.67 No.10: 3169–3185
https://doi.org/10.1007/s11430-024-1368-0

# Chemical, carbon and sulfur isotopic compositions constrain the origin of Upper Carboniferous-Lower Triassic gases in eastern Sichuan Basin, SW China

Chunfang CAI[1,2,4*], Ilya KUTUZOV[3], Wenhua MEI[2,4], Daowei WANG[5], Bing LUO[6], Shipeng HUANG[7], Bing HE[6] & Alon AMRANI[3]

[1] *China University of Petroleum, National Key Lab Petroleum Resource & Engineering, Beijing 102249, China;*
[2] *State Key Laboratory of Lithospheric and Environmental Coevolution, Institute of Geology and Geophysics, Chinese Academy of Sciences, Beijing 100029, China;*
[3] *Institute of Earth Sciences, The Hebrew University, Jerusalem 91904, Israel;*
[4] *College of Earth and Planetary Sciences, University of Chinese Academy of Sciences, Beijing 100049, China;*
[5] *Yulin University, Yulin 719000, China;*
[6] *Research Institute of Exploration and Development, Southwest Oil & Gas Field Company, PetroChina, Chengdu 610051, China;*
[7] *PetroChina, Research Institute of Petroleum Exploration and Development, Beijing 100083, China*

Received February 21, 2024; revised June 11, 2024; accepted June 24, 2024; published online September 4, 2024

**Abstract** Methane dominated gas is one of the cleanest energy resources; however, there is no direct method to determine its source rock. Natural gases produced from the eastern Sichuan Basin together with seismic data were studied for their sources and secondary alteration by thermochemical sulfate reduction (TSR). Our results demonstrate that Upper Permian to Lower Triassic ($P_3$ch-$T_1$f) gases in the surrounding of the Kaijiang-Liangping area show volatile organic sulfur compounds (VOSCs) $\delta^{34}$S values close to those of the associated $H_2S$, and may have been altered by methane-dominated TSR, resulting in positive shift in methane $\delta^{13}C_1$ values with increasing TSR extents. Other (or group 2) gases produced from the $P_3$ch-$T_1$f reservoirs from the southern area and the Upper Carboniferous to Middle Permian ($C_2$h-$P_2$q) from the eastern Sichuan Basin are not significantly changed by TSR, show similar $\delta^{34}$S values between the kerogens and some VOSCs, and may have been derived from the Lower Silurian and Middle Permian source rocks. This study demonstrates a case for the first time showing the $\delta^{34}$S values of VOSCs can be used as a tool for direct correlation between non-TSR altered gas and source rocks. Methane-dominated gas pools can be found using gas and source rock geochemistry combined with seismic data.

**Keywords** Sulfur isotopes, Volatile organic sulfur compounds, Thermochemical sulfate reduction, Sichuan Basin, Gas-source rock correlation

**Citation:** Cai C, Kutuzov I, Mei W, Wang D, Luo B, Huang S, He B, Amrani A. 2024. Chemical, carbon and sulfur isotopic compositions constrain the origin of Upper Carboniferous-Lower Triassic gases in eastern Sichuan Basin, SW China. Science China Earth Sciences, 67(10): 3169–3185, https://doi.org/10.1007/s11430-024-1368-0

## 1. Introduction

Natural hydrocarbon gas, especially methane dominated gas with C:H molar ratio of 1:4, is one of the cleanest energy resources, and it is important to determine its source rock for the exploration. Hydrocarbon gas includes biogenic gas generated through low temperature (<80°C) microbial degradation at vitrinite reflectance *R*o<0.5%, and thermogenic gas generated from thermal cracking of organic matter or kerogen with *R*o from 0.6% to 3.0%. Oil-associated gas is

* Corresponding author (email: cai_cf@mail.iggcas.ac.cn)

generated from thermally mature organic matter, and wet gas and dry gas from the overmature stages. Molecular and carbon isotopic compositions of a hydrocarbon gas are controlled by organic matter types and $\delta^{13}C$ values, and organic matter maturity, and are thus routinely used to reflect its genesis (Schoell, 1980; James, 1983; Galimov, 1988; Behar et al., 1991; Berner and Faber, 1996). Biogenic gases can be distinguished from abiogenic gases using $C_1/(C_2+C_3)$ ratios and methane $\delta^{13}C_1$ diagrams, and relationships among $\ln(C_1/C_2)$, $\ln(C_2/C_3)$, $\delta^{13}C_2$-$\delta^{13}C_1$ and $\delta^{13}C_3$-$\delta^{13}C_2$ are used to differentiate primary kerogen-cracking gas from the secondary oil-cracking gas (Behar et al., 1991; Whiticar, 1994; Prinzhofer et al., 2000), but there is no direct proxy to determine the source rock of natural gases.

Natural hydrocarbon gas in oil and gas fields is generally associated with volatile organic sulfur compounds (VOSCs) including thiols, sulfides and thiophenes, despite of their low concentrations (0.1 ppm to tens ppm, 1 ppm=1 μg/g), and with $H_2S$ with high concentrations (>20% in volume) in some gas pools. $H_2S$ is toxic and strongly caustic, and thus it is necessary to adopt anticaustic material if $H_2S$ distribution can be determined prior to drill for petroleum pools. VOSCs and $H_2S$ can be generated from bacterial sulfate reduction (BSR), thermochemical sulfate reduction (TSR), or thermal cracking alteration (TCA) of organic matter such as kerogen and crude oil (Cai et al., 2003; Amrani et al., 2019; Xiao et al., 2021; Kutuzov et al., 2023b; Souza et al., 2022). BSR and TSR are redox reactions between hydrocarbons and dissolved sulfate in <102°C and >120°C, respectively, to generate $H_2S$, $CO_2$ and organic sulfur compounds as the reaction products (Orr, 1974; Krouse et al., 1988; Elsgaard et al., 1994; Cai et al., 2009b, 2016). Gases derived from kerogen thermal cracking are proposed to be enriched in thiols, sulfides, and thiophenes, while a BSR source is primarily composed of thiols with limited sulfides and thiophenes (Xiao et al., 2021). Thiols from the Triassic in the Sichuan Basin were proposed to have been generated from the incorporation of TSR-derived $H_2S$ into hydrocarbons (Cai et al., 2003). Simulation experiments support the formation of thiols and sulfides by $H_2S$ reactions with hydrocarbons (Meshoulam and Amrani, 2017; Amrani et al., 2019). The thermally labile thiols, thiolanes and sulfides are found to be rapidly generated accompanied by their decomposition during TSR stage (Amrani et al., 2008; Cai et al., 2022).

It is generally accepted that there is no significant sulfur isotope fractionation during TSR in petroleum reservoirs as the result of complete reduction of any dissolved sulfate and anhydrite dissolution as the rate-limiting step during TSR but large fractionation takes place during BSR (Orr, 1974; Machel et al., 1995; Bildstein et al., 2001). Sulfur compounds, including VOSCs that are generated from closed-system pyrolysis of kerogen or naturally produced in petroleum basins are found to have mostly similar isotopic compositions (<2‰–5‰) to the parent kerogen, thus sulfur isotopic compositions ($\delta^{34}S$) can be used for the correlations between oil and source rock and potentially between gas and source rock (Orr, 1986; Idiz et al., 1990; Amrani et al., 2005, 2019; Cai et al., 2009a, 2015, 2017b; Rosenberg et al., 2017; Greenwood et al., 2018; Kutuzov et al., 2023b).

During interaction with $H_2S$ (e.g., from TSR), the less stable VOSCs such as thiols will rapidly change their $\delta^{34}S$ values towards the $H_2S$ in the reservoir, and will be controlled by equilibrium isotopic effect (EIE) with the associated TSR-$H_2S$, as demonstrated by the cases from the Ordos and Alberta Basins, and from experimental simulation (Amrani et al., 2019; Kutuzov et al., 2021, 2023a, 2023b).

Thus, concentrations and isotopic compositions of $H_2S$, $CO_2$ and other inorganic and organic sulfur species are used to distinguish their generation from TSR, BSR or TCA processes, and to determine what kind of the organic matter involved and its sources (Worden and Smalley, 1996; Gvirtzman et al., 2015; Cai et al., 2016, 2022; Meshoulam et al., 2016; Kutuzov et al., 2023b). So far, gas-source rock correlation was preformed only in Ordos Basin using sulfur isotopic compositions of thiophenes based on, (1) laboratory experiments showing $\delta^{34}S$ value of thiophenes from thermal cracking of a kerogen follows that of the parent kerogen, and (2) sulfur isotopic compostions of thiophenes from the Alberta and Ordos Basins gases are not in isotopic equilibrium with the associated TSR-derived $H_2S$. However, in these two cases, the gases are heavily altered by interaction with $H_2S$; in the Ordos basin, all the VOSCs except six sulfides show $\delta^{34}S$ values from +28‰ to +34‰ (Kutuzov et al., 2023a), which are similar to or even higher than those of Ordovician anhydrite with $\delta^{34}S$ values from +25.8‰ and +28.0‰ with a mean value of +27.5‰ ($n$=8; Cai et al., 2005) and the coeval seawater sulfate (Claypool et al., 1980). Thus, it is not clear if the thiophenes that are not in equilibrium with the associated $H_2S$ were totally derived from source rock kerogen, or the thiophenes have mixed with TSR-derived thiophenes. In addition, source rock kerogen is generally shown to have $\delta^{34}S$ values 5‰ to 15‰ lighter than that of the coeval seawater from which organic matter deposited (Cai et al., 2009a, 2009b; Amrani, 2014). However, the Ordovician source rock in the Ordos Basin kerogen has been considered to have a $\delta^{34}S$ value similar to the coeval seawater based on a single source rock sample measurement, it is required to provide more data. VOSCs were also measured for $\delta^{34}S$ values in the Alberta Basin, where thiophenes were used for gas-oil correlation.

Gases from the eastern Sichuan Basin produced from the Upper Permian to Lower Triassic are proposed to have been altered by TSR, resulting in significantly positive shift in $\delta^{13}C_1$ (Cai et al., 2003, 2004, 2013; Liu et al., 2013; Li et al., 2019). Hu et al. (2014) proposed that the Upper Permian Longtan Formation ($P_3l$) coal is the main source rock in

Kaijiang-Liangping area based on carbon isotopes of kerogen, solid bitumen and ethane. Cai et al. (2017a, 2017b) considered $P_3$l mudstone with type II kerogen as the source rock of the gases based on limited sulfur isotopic compositions and biomarkers of solid bitumen and source rocks. More recently, natural gases are found from the Middle Permian Qixia ($P_2$q) and Maokou ($P_2$m) formations and estimated to have an inferred resource amount of about $14{,}700\times10^8$ $m^3$ and a proven reserve of $810\times10^8$ $m^3$ (Wang et al., 2018), and are proposed, but not proven, to have been derived from the Lower Silurian source rocks with a small contribution from the Middle Permian source rocks based on the similarity of parent kerogen, ethane $\delta^{13}C$ values, and petroleum charge history analysis (Li et al., 2021; Huang et al., 2023). In contrast, the gases produced from Maokou Formation Member 1 in the Fuling area, eastern Sichuan Basin, are considered to have been derived from the Middle Permian source rocks based on the empirical relationship, i.e., kerogen $\delta^{13}C$ values are about 3‰ heavier than that of the produced methane (Hu D F et al., 2020).

In this contribution, we analyzed eastern Sichuan Basin gases for chemical compositions, volatile organic sulfur compounds (VOSCs) $\delta^{34}S$ values, and alkanes $\delta^{13}C$ and $\delta^{2}H$ values. We aim to: (1) distinguish TSR-altered gases from the non-TSR gases using gas souring index, VOSCs compositions and their $\delta^{34}S$ values; (2) develop a direct method (sulfur isotope proxy) along with alkanes $\delta^{13}C$ and $\delta^{2}H$ values to determine the source rock of non or minor TSR natural gases.

## 2. Geologic settings

### 2.1 Stratigraphy and structure

The Sichuan Basin in southwest China is one of China's largest natural gas provinces with gas found in the Triassic, Permian, Carboniferous, Cambrian and Upper Ediacaran (Cai et al., 2003; Hu Y J et al., 2020; Liu et al., 2021). The eastern part of the Sichuan Basin, located on the northern margin of the Yangtze Plate, exhibits a NE-trending belt-like distribution (Figure 1a). This area belongs to the high and steep tectonic zone of eastern Sichuan, adjacent to the Daba Mountain foreland thrust belt (He et al., 2011). From the Late Cambrian to the Middle Permian, sedimentation in the northeastern area of eastern Sichuan is dominated by shallow marine carbonates and black shale (Cai et al., 2003). The Dongwu Orogeny during the late period of Middle Permian caused the uplift and erosion of the Yangtze craton. During the Late Permian, a marine transgression occurred in the study area, forming the Kaijiang-Liangping Trough. This transgression led to the development of slope transition facies and marginal reefs, which provided favorable conditions for natural gas accumulation (He et al., 2011). As a result of the Indosinian Orogeny between the Middle and Upper Triassic, the Sichuan Basin was uplifted and exposed, and seawater was retreated from the basin. After then, 2000–5000 m thick Upper Triassic to Cretaceous freshwater lacustrine-alluvial clastics with local coal beds were deposited (Figure 1b). The present numerous thrust faults and anticline structures of the study area were formed during the Yanshan and Himalayan orogenies from late Cretaceous to Eocene as the result of strong compression from north to south and from east to west.

### 2.2 Source rocks and hydrocarbon generation history

Potential source rocks for the Permian to Lower Triassic gas reservoirs in the basin include Lower Silurian Longmaxi Formation ($S_1$l) mudstone and shale, Middle Permian Qixia ($P_2$q) and Maokou ($P_2$m) formations, Upper Permian Longtan Formation ($P_3$l) and Upper Permian Dalong Formation ($P_3$d), which is isochronous with Changxing Formation ($P_3$ch) dolostones (Figure 1b). The $S_1$l source rock is 40–80 m thick black shale and dark gray mudstone, has TOC of more than 2.0 wt.%, and shows type-I to type-II kerogen and an average equivalent vitrinite reflectance ($Ro_{equ.}$) of about 2.6% which is calculated from solid bitumen reflectance ($R$b) (Cai et al., 2017b).

Both the $P_2$m and $P_2$q source rocks are argillaceous limestone with type II–I kerogen and have $Ro_{equ.}$ of 2.1% to 2.7%, with thickness of 30–220 m and TOC of 0.2%–3.0% (averaged at 0.86%) and 10–70 m thick and TOC of 0.5%–2.0% for $P_2$m and $P_2$q Formation source rock, respectively (Huang et al., 2016; Hu D F et al., 2020). The $P_3$l Formation source rocks include marine-terrigenous transitional facies laminar coal seams and terrigenous mudstone with type II to III kerogen and restricted deep water shelf facies sapropelic-dominated mudstones in the Bazhong-Dazhou depression in the northern Sichuan Basin (Cai et al., 2017a) . This suite of source rock has TOC from 0.64% to 10.8% with an average of 2.06% and thickness from 40 m to 140 m (Cai et al., 2017b).

Based on burial-thermal history rebuilding on NE Sichuan Basin (Figure 2; Li et al., 2021), peak oil and gas generation from the Lower Silurian source rocks occurred during the Late Permian to Early Triassic and the late Triassic to Jurassic, respectively; and peak gas was generated from the Middle Permian source rock during the Jurassic to Early Cretaceous.

## 3. Sampling and methods

A total of nineteen gas samples were collected from the Carboniferous, Permian and Triassic reservoirs of eastern Sichuan Basin (Figure 1a), including four gas samples from Feixianguan Formation ($T_1$f), eight from Changxing For-

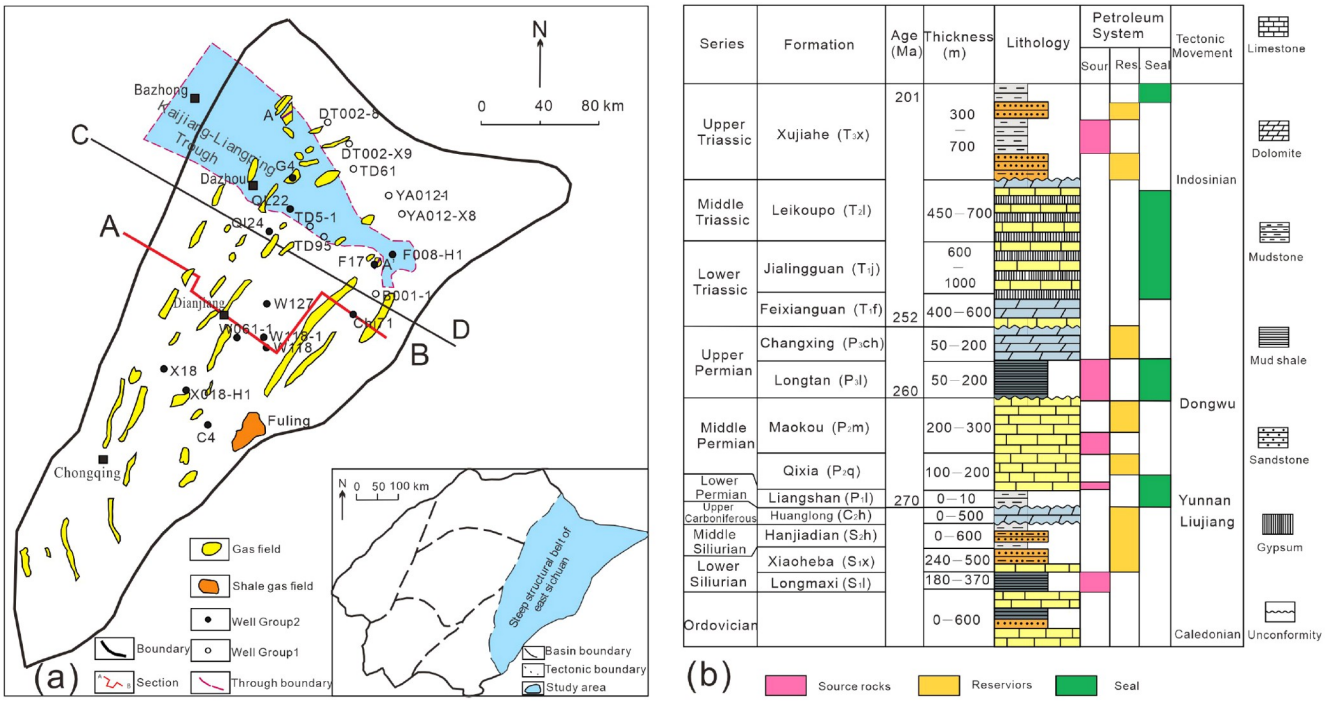


**Figure 1** Diagrams showing distribution of natural gas pools and locations of sampling wells in eastern Sichuan with insets for maps of the Sichuan Basin (a), and generalized stratigraphic column showing complex distribution of source rocks, reservoirs and seal rocks (b) (modified from Huang et al., 2023). Line AB is the seismic line in Figure 11 and line CD divides southern and northern eastern Sichuan Basin.

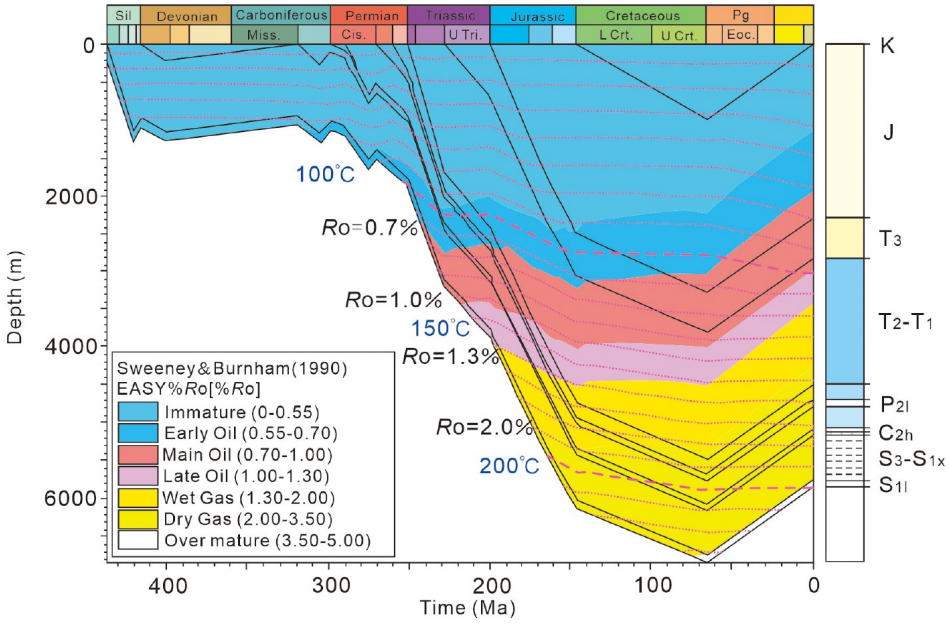


**Figure 2** Burial and thermal evolution history rebuilding of hydrocarbon generation in the eastern Sichuan Basin (Li et al., 2021).

mation ($P_3$ch), three from Maokou Formation ($P_2$m), one from the Qixia Formation ($P_2$q) and three from the Upper Carboniferous ($C_2$h). These samples were collected directly from the wellhead into both 1.5 L Teflon-lined stainless-steel cylinders and 75 mL Swagelok passivated cylinders (Sulfinert®) before air pollution removal through flushing. After the gas samples were collected, each cylinder was immersed in water for leak testing. The samples in the stainless steel cylinders were transported to the Northwest Institute of Eco-Environment and Resources, Chinese Academy of Sciences (Lanzhou city, NW China) for analyses of chemical and carbon and hydrogen isotopic composition. The other gas samples, in Swagelok passivated cylinders (Sulfinert®) were transported to the Hebrew University of Jerusalem, Israel

(HUJI) for the analyses of VOSCs concentrations and their $\delta^{34}S$ values.

### 3.1 Chemical composition of natural gas

The molecular compositions of gas samples were analyzed by combining a isotope mass spectrometer with gas chromatography (Cao et al., 2016) in the Oil and Gas Research Center, Northwest Institute of Eco-Environment and Resources (NIEER), Chinese Academy of Sciences in Lanzhou city. Individual hydrocarbon gas components ($C_1$ to $C_5$) were analyzed by an Agilent 6890 N gas chromatograph equipped with a flame ionization detector and a capillary column (PLOT $Al_2O_3$ 50 m×0.53 mm). The GC oven temperature started at 30°C (10 min) and was programmed to 180°C at 10°C/min, and then held at this temperature for 20–30 min. Non-hydrocarbon gases were determined on a Finnigan MAT-271 mass spectrometer (Reber and Cordes, 1995). Operating conditions were: ion source, 95°C; emission current, 40 μA; electron energy, 86 eV; mass scan range, 1 to 70 amu and injection volume, 1 mL. The concentration of each component was calculated using the calibration curve obtained from standard gases. The non-hydrocarbon component data from the mass spectrometer and the hydrocarbon gas component ($C_1$ to $C_5$) data from the gas chromatograph were normalized to obtain the final full component data results. Among the samples, fourteen samples were re-analyzed after one and half year at HUJI and show similar values except sample TD5-1 with some $H_2S$ in the earlier analysis but no detectable $H_2S$ during the later analysis Tables S1 and S2, https://link.springer.com). Considering that no VOSCs were detected from this sample, no significant $H_2S$ is expected and thus the result from the later analysis is used. The gas chromatograph (GC; Agilent 7890B) was equipped with sulfinert lines and inlet, three pneumatic Hastelloy valves, four 1/8" nickel-packed columns and a TCD detector designed for sour gas analysis to determine the components and concentrations of hydrocarbons and non-hydrocarbon gases ($N_2$, $CO_2$ and $H_2S$). The GC oven was programmed to remain at 90°C for 25 min while the sample was diverted between the different columns with a pre-set program. The gas chromatograph was calibrated using a certified standard gas mixture (G3440-85017; Agilent Technologies, DE, USA) which contains $C_1$–$C_5$ hydrocarbons and non-hydrocarbon gases ($CO_2$, $N_2$, He) commonly occurring in natural gas reservoirs. Quantification of $H_2S$ was performed against two lab-made standard mixtures of $H_2S$ (1.1% and 12.9%) in natural gas from the Mediterranean (99% methane, no VOSC traces) used by Meshoulam et al. (2021). Considering that propane to pentane compounds were detected only from the earlier analysis and thus the earlier results with their carbon isotopic compositions (Tables S1 and S2) are discussed in this contribution.

### 3.2 Carbon and hydrogen isotopes of alkanes

A Thermo Finnigan Delta V Advantage mass spectrometer interfaced to an Trace 1310 gas chromatograph was employed to determine stable carbon and hydrogen isotope ratios. The carbon isotope GC conditions were as follows: HP-PLOT-Q column (30 m×0.53 mm×40 μm); He (99.999%) carrier gas at a flow rate of 3.0 mL/min, the GC oven temperature started at 50°C (3 min) and then increased to 200°C at 15°C/min and held at 200°C for 20 min. The hydrogen isotope GC conditions were as follows: HP-$Al_2O_3$/KCl column (50 m×0.53 mm×10 μm), helium carrier gas at a flow rate of 3.0 mL/ min, the GC oven was held constant at 45°C for 3 min and then heated to 200°C at a rate of 15°C/min and held at 200°C for 20 min. All samples were injected in split mode with a split ratio of 6 and the injector temperature was 200°C..

### 3.3 VOSC composition and sulfur isotopes

Fourteen samples were analyzed for VOSCs concentrations and isotopic compositions using the same methods as reported by Said-Ahmad et al. (2017) and Kutuzov et al. (2023a). In brief, the system employed a modified GC (GC 7890, Agilent Technologies, CA, USA) with passivated tubing (Sulfinert®) in combination with a TCD or with the Neptune Plus™ MC-ICPMS (ThermoScientific, Germany). The GC was equipped with a heated (70°C) six-way valve gas inlet system (Valco Instrument Co, TX, USA) to introduce gaseous compounds through a computer-controlled actuator. A Deans Switch (Agilent Technologies, CA, USA) connected to the GC column performs heart cutting for selected peaks ($H_2S$ and COS) so that both VOSCs as low as sub-ppm levels and percent-level $H_2S$ can be analyzed. Helium was used as a carrier gas to transfer the analytes from the GC through a fused-silica capillary into the Neptune ion source. The effluent from the GC column (DB-Sulfur SCD column, 60 m×0.32 mm×4.2 μm, methyl-deactivated, Agilent Technologies) was diverted either to the TCD or to the MC-ICPMS via a heated transfer line (~200°C). SF6 gas (in helium) was used for calibration and was injected at the beginning and end of each sample analysis by a laboratory-built SF6 reference gas injector with a six-way valve (Amrani et al., 2009). Each gas sample was measured at least twice. Precision and accuracy were typically better than 0.5‰ but in a single case reached up to 1.1‰. $H_2S$ was measured for $\delta^{34}S$ values by first passing the gas through $AgNO_3$ solution (5%) to precipitate $Ag_2S$, which was then measured by a continuous-flow method using a Flash EA 1112 series elemental analyzer coupled to a Delta Plus mass spectrometer (ThermoFinnigan, Germany) following Giesemann et al. (1994) and Shawar et al. (2020). The $\delta^{34}S$ values of $H_2S$ are averages of at least 2 replicate analyses

($n$≥2) with precision better than 0.3‰. The $\delta^{34}S$ values were calibrated using a calibration curve with the international standards NBS-127, IAEA-S-1, and IAEA–SO–6.

## 4. Result

### 4.1 Chemical composition and $\delta^{13}C$ and $\delta^{2}H$ values

The gases have methane content ranging from 88.9% to 99.1%, dryness coefficient ($C_1/C_{1\text{-}5}$) from 0.948 to 0.999, $H_2S$ and $CO_2$ contents from 0 to 4.9% and 0 to 2.6%, respectively, and gas souring index $100\times(H_2S+CO_2)/(H_2S+CO_2+C_{1\text{-}5})$ (or GSI) from 0 to 5.5 (Table 1). Gases with detectable $H_2S$ or GSI>0.9 are exclusively produced from the $P_3$ch and $T_1$f. These gases can be divided into two groups. Group 1 gases are exclusively sampled from the $P_3$ch and $T_1$f reservoirs in the surroundings of and north to the Kaijiang-Liangping trough, and group 2 are from $C_2$h and $P_2$m reservoirs in the eastern Sichuan Basin and $P_3$ch to $T_1$f reservoirs from the south to the Kaijiang-Liangping trough. It is clear that group 1 gases show a positive correlative relationship between GSI and $C_1/C_{1\text{-}5}$ ratios with correlation coefficient $R^2$ of 0.57 (Figure 3a).

The gases show wide variations in methane $\delta^{13}C_1$ and $\delta^{2}H$ values, ranging from −34.2‰ to −30.0‰ and −137.8‰ to −123.6‰, respectively (Figure 4a; Table 2), and have ethane $\delta^{13}C_2$ from −37.0‰ to −22.7‰ ($n$=19), propane $\delta^{13}C_3$ from −38.7‰ to −19.0‰ ($n$=13), and carbon dioxide $\delta^{13}C_{CO2}$ from −5.5‰ to +0.7‰ ($n$=15). The $\delta^{13}C_2$ values range from −36.8‰ to −31.7‰ for the $T_1$f gases, from −37.0‰ to −22.7‰ for the $P_3$ch gases, from −35.6‰ to −22.7‰ for the $P_2$m and $P_2$q gases, and from −36.8‰ to −35.2‰ for the $C_2$h gases. The group 1 gases show positive relationships of $\delta^{13}C_1$ to both GSI (Figure 3b) and $\delta^{13}C_2$ (Figure 4b) with $R^2$ of 0.47, but no correlative relationship for all the gases and the group 2 gases, respectively. $\delta^{13}C_3$ values for the $T_1$f gases range from −38.7‰ to −23.4‰, from −35.8‰ to −19.0‰ for the $P_3$ch gases, −29.4‰ for a $P_2$m gas, and are not available for the $C_2$h gases. There exists a roughly positive correlation between $\delta^{13}C_2$ and $\delta^{13}C_3$ values (Figure 4c). The majority of the gas samples, i.e., 16 among the 19 gases, shows carbon isotope reversal for methane and ethane ($\delta^{13}C_1\geqslant\delta^{13}C_2$), but normal sequence for ethane, propane and butane with 12 among 13 gases showing $\delta^{13}C_2\leqslant\delta^{13}C_3$, and 1 among the 10 gases showing $\delta^{13}C_3<\delta^{13}C_4$ (Figure 5).

Although the least negative $\delta^{13}C_1$ value of −30.0‰ found in the sample YA012-1 from the group 1 showing the highest TSR extent (Figure 3b), similarly heavy $\delta^{13}C_1$ values are also

**Table 1** Chemical compositions and their ratios of the natural gas samples from Northeastern Sichuan Basin[a)]

| Group | Well | Formation | $nC_1$ | $nC_2$ | $nC_3$ | $iC_4$ | $nC_4$ | $CO_2$ | $N_2$ | $H_2S$ | $C_1/C_{1\text{-}5}$ | GSI (%) | TSR or not |
|---|---|---|---|---|---|---|---|---|---|---|---|---|---|
| 1 | TD95 | $T_1$f | 96.91 | 0.49 | 0.04 | 0.00 | 0.00 | 0.03 | 2.20 | 0.00 | 0.995 | 0.028 | None |
| 1 | TD5-1 | $T_1$f | 96.80 | 0.20 | 0.02 | 0.00 | 0.00 | 2.60 | 0.40 | 0.00 | 0.998 | 2.680 | None |
| 1 | DT002-8 | $P_3$ch | 97.34 | 0.22 | 0.01 | 0.00 | 0.00 | 0.04 | 2.05 | 0.00 | 0.998 | 0.038 | None |
| 1 | DT002-X9 | $P_3$ch | 88.89 | 0.13 | 0.00 | 0.00 | 0.00 | 0.05 | 6.59 | 2.81 | 0.999 | 3.216 | TSR |
| 1 | TD61 | $P_3$ch | 95.07 | 0.36 | 0.03 | 0.00 | 0.00 | 0.05 | 2.93 | 0.93 | 0.996 | 1.031 | TSR |
| 1 | B001-1 | $P_3$ch | 94.81 | 0.14 | 0.00 | 0.00 | 0.00 | 0.09 | 2.45 | 2.21 | 0.999 | 2.415 | TSR |
| 1 | YA012-1 | $P_3$ch | 92.55 | 0.08 | 0.00 | 0.00 | 0.00 | 0.17 | 2.24 | 4.90 | 0.999 | 5.479 | TSR |
| 1 | YA012-X8 | $P_3$ch | 93.09 | 0.09 | 0.00 | 0.00 | 0.00 | 0.25 | 3.88 | 2.26 | 0.999 | 2.700 | TSR |
| 2 | X018-H1 | $T_1$f | 98.81 | 0.42 | 0.07 | 0.01 | 0.01 | 0.01 | 0.61 | 0.00 | 0.995 | 0.006 | None |
| 2 | W061-1 | $P_3$ch | 94.27 | 3.56 | 1.03 | 0.37 | 0.19 | 0.08 | 0.00 | 0.00 | 0.948 | 0.086 | None |
| 2 | W118-1 | $P_3$ch | 97.66 | 0.42 | 0.05 | 0.01 | 0.01 | 0.01 | 1.45 | 0.00 | 0.995 | 0.000 | None |
| 2 | W118 | $P_2$m | 99.13 | 0.29 | 0.02 | 0.00 | 0.00 | 0.01 | 0.46 | 0.00 | 0.997 | 0.009 | None |
| 2 | G4 | $P_2$m | 94.75 | 0.30 | 0.01 | 0.00 | 0.00 | 0.00 | 3.83 | 0.00 | 0.997 | 0.007 | None |
| 2 | QL22 | $P_2$m | 97.27 | 0.18 | 0.01 | 0.00 | 0.00 | 0.00 | 1.37 | 0.75 | 0.998 | 0.768 | TSR |
| 2 | QL24 | $C_2$h | 98.61 | 0.20 | 0.01 | 0.00 | 0.00 | 0.06 | 1.03 | 0.00 | 0.998 | 0.061 | None |
| 2 | Feng008-H1 | $C_2$h | 99.08 | 0.45 | 0.02 | 0.00 | 0.00 | 0.01 | 0.35 | 0.00 | 0.995 | 0.011 | None |
| 2 | Feng17 | $C_2$h | 98. 10 | 0.37 | 0.03 | 0.00 | 0.00 | 0.01 | 1.38 | 0.00 | 0.996 | 0.010 | None |
| 2 | Cao4 | $T_1$f | 98.58 | 0.77 | 0.19 | 0.04 | 0.05 | 0.02 | 0.16 | 0.00 | 0.989 | 0.018 | None |
| 2 | W127 | $P_2$q | 94.67 | 0.21 | 0.01 | 0.00 | 0.00 | 0.08 | 3.73 | 0.44 | 0.998 | 0.554 | TSR |

a) GSI is $100\times(H_2S+CO_2)/(H_2S+CO_2+C_{1\text{-}5})$

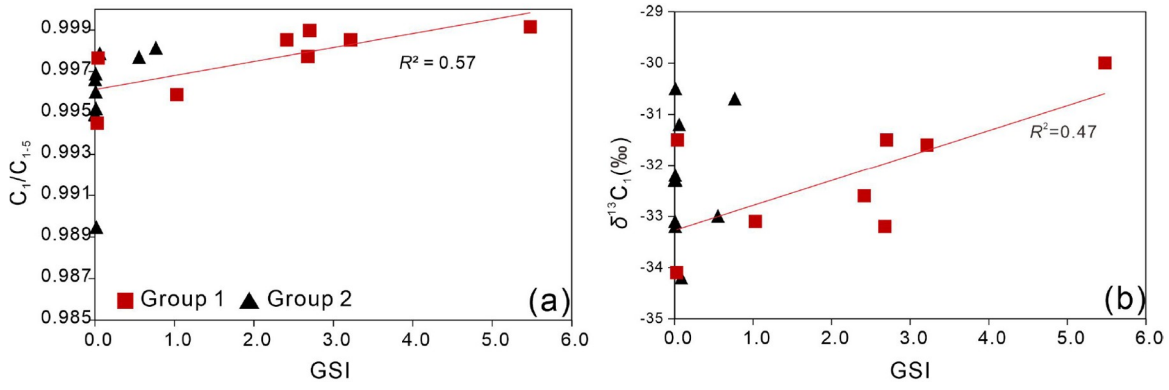


**Figure 3** Relationships of gas sourcing index GSI (or $100\times(H_2S+CO_2)/(H_2S+CO_2+\Sigma C_{1\text{-}5})$) to dryness coefficient ($C_1/C_{1\text{-}5}$) (a) and methane $\delta^{13}C_1$ (b), showing roughly positive correlative relstionships for the group 1 gases, but not for group 2 gases.

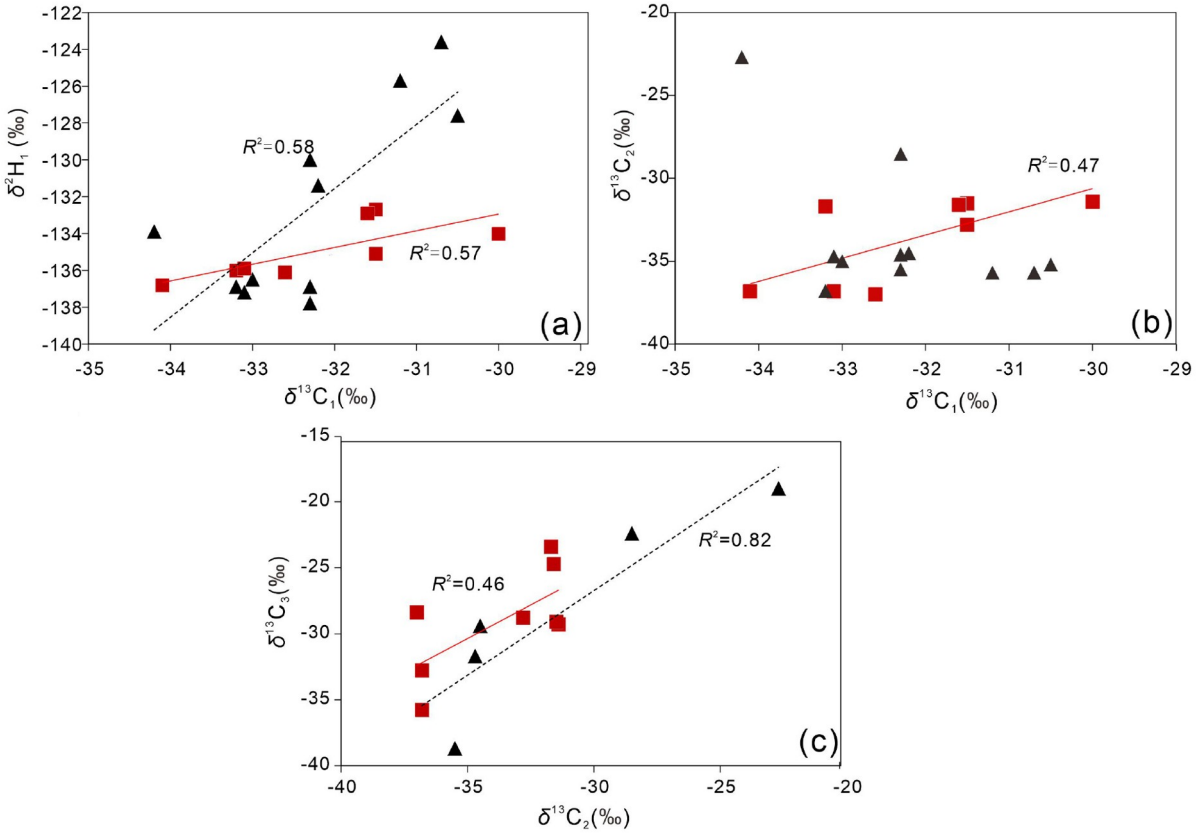


**Figure 4** Diagrams of (a) methane $\delta^{13}C_1$ against $\delta^2H_1$, (b) $\delta^{13}C_1$ against $\delta^{13}C_2$, and (c) $\delta^{13}C_2$ against $\delta^{13}C_3$, showing that roughly positive correlative relstionships of $\delta^{13}C_1$ vs $\delta^2H_1$ and $\delta^{13}C_2$ vs $\delta^{13}C_3$ for both the two group gases, respectively.

distributed in group 2 gases without significant amount of associated $H_2S$. The least negative $\delta^{13}C_2$ value of −22.7‰ is found in sample W061-1 with no detectable $H_2S$.

### 4.2 Volatile organic sulfur compounds (VOSCs) and $H_2S$ and their $\delta^{34}S$ values

VOSCs are present in 7 samples out of the 14 gases analyzed with concentrations ranging from 1.7 ppm to 135.8 ppm ($n$=7; Table 3). All the samples were dominated by thiols (1.7–133.7 ppm; Figure 6), with methanethiol (MeSH) being the predominant thiol in all samples (0.9–99.8 ppm). Organic sulfides are present in all the samples except TD61, and mainly composed of dimethylsulfide (DMS) and dimethyl disulfide (DMDS), and have concentrations from 0.1 to 8.7 ppm. Thiophene was detected only in samples YA012-1 and DT002-X9 at trace concentrations of 0.1 ppm and 0.2 ppm, respectively.

Compound specific sulfur isotopes analysis of the VOSC demonstrates that five samples have VOSCs dominated by

**Table 2** Carbon isotopic compositions of alkanes and $CO_2$ of the natural gas samples[a)]

| Group | Well | Formation | $\delta^{13}C$ (‰) | | | | | | $\delta^{2}H$ (‰) |
|---|---|---|---|---|---|---|---|---|---|
| | | | $CH_4$ | $C_2H_6$ | $C_3H_8$ | $iC_4H_{10}$ | $nC_4H_{10}$ | $CO_2$ | $CH_4$ |
| 1 | TD95 | $T_1f$ | −34.1 | −36.8 | −32.8 | −29.6 | −26.7 | −0.6 | −136.8 |
| 1 | TD5-1 | $T_1f$ | −33.2 | −31.7 | −23.4 | −20.1 | −18.5 | −5.5 | −136.0 |
| 1 | DT002-8 | $P_3ch$ | −31.5 | −32.8 | −28.8 | – | – | −0.4 | −132.7 |
| 1 | DT002-X9 | $P_3ch$ | −31.6 | −31.6 | −24.7 | – | −18.4 | −2.4 | −132.9 |
| 1 | TD61 | $P_3ch$ | −33.1 | −36.8 | −35.8 | – | −29.4 | −3.1 | −135.9 |
| 1 | B001-1 | $P_3ch$ | −32.6 | −37.0 | −28.4 | – | −27.4 | −2.1 | −136.1 |
| 1 | YA012-1 | $P_3ch$ | −30.0 | −31.4 | −29.3 | – | – | −0.3 | −134.0 |
| 1 | YA012-X8 | $P_3ch$ | −31.5 | −31.5 | −29.1 | – | – | 0.5 | −135.1 |
| 2 | X018-H1 | $T_1f$ | −33.1 | −34.7 | −31.7 | −29.3 | −27.8 | – | −137.2 |
| 2 | W061-1 | $P_3ch$ | −34.2 | −22.7 | −19.0 | −18.5 | −15.6 | 0.7 | −133.9 |
| 2 | W118-1 | $P_3ch$ | −32.3 | −28.5 | −22.4 | −18.5 | −29.1 | −0.3 | −137.8 |
| 2 | W118 | $P_2m$ | −32.2 | −34.5 | −29.4 | – | −26.5 | −1.4 | −131.4 |
| 2 | G4 | $P_2m$ | −32.3 | −34.6 | – | – | – | – | −130.0 |
| 2 | QL22 | $P_2m$ | −30.7 | −35.6 | – | – | – | – | −123.6 |
| 2 | QL24 | $C_2h$ | −31.2 | −35.7 | – | – | – | 0.0 | −125.7 |
| 2 | Feng008-H1 | $C_2h$ | −30.5 | −35.2 | – | – | – | 0.7 | −127.6 |
| 2 | Feng17 | $C_2h$ | −33.2 | −36.8 | – | – | – | −2.4 | −136.9 |
| 2 | Cao4 | $T_1f$ | −32.3 | −35.5 | −38.7 | −26.5 | −27.8 | – | −136.9 |
| 2 | W127 | $P_2q$ | −33.0 | −35.0 | – | – | – | −1.0 | −136.5 |

a) –, no data available

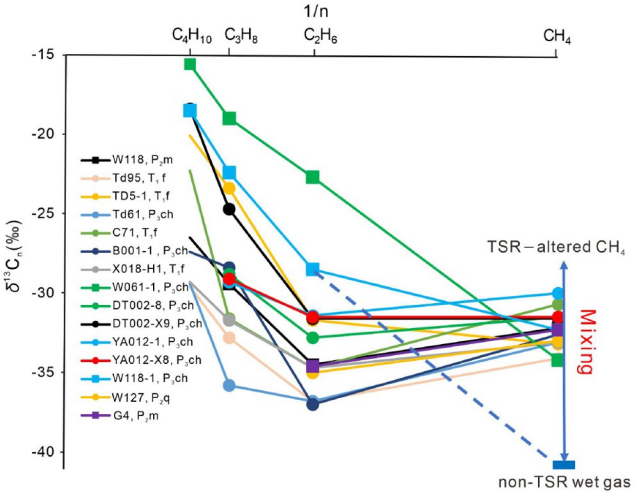


**Figure 5** Alkanes $\delta^{13}C_n$ vs. $1/n$ diagram showing that the most of the gases have methane $\delta^{13}C_1$ significantly heavier than the co-generative, unaltered gas of the Chung et al. (1988)'s model, indicating mixing with $^{13}C$-rich methane.

$\delta^{34}S$ values higher than +15.0‰. Other two gases from the TD61 and W118 wells have propanethiols (PrSH) $\delta^{34}S$ values from +17.0‰ to +23.2‰, and MeSH and ethanethiol (EtSH) from +10.6‰ to +14.7‰ (Figure 7), and have the lightest values of +8.7‰ for DMDS and +8.8‰ for an unknown sulfur-bearing compound. The $\Delta^{34}S$ between the lightest and heaviest thiol in the different samples varied between 0.0‰ to 7.8‰ depending on the sample. Sulfides were present in all samples except TD-61 and covered an isotopic range of +14.1‰ to +25.0‰. In general, sulfides were both isotopically lighter and heavier by several per mil when compared to the thiols in all the samples except DT002-X9. Sample DT002-X9 had $CH_3SSH$ as its only detectable sulfide, and it had $\delta^{34}S$ of +15.5‰ which is 3.0‰ heavier than the 2-BuSH but lighter than all other thiols in the sample. The $\Delta^{34}S$ between the lightest and heaviest sulfide in the different samples vary between 6.6‰ to 10.2‰ depending on the sample. Only two samples DT002-X9 and YA012-1 had sufficient thiophene for isotopic analysis, which had $\delta^{34}S$ values of +20.0‰ and +29.3‰, respectively. These values are the heaviest among those of all the VOSCs in the samples. Among these samples, four were analyzed for $H_2S$ $\delta^{34}S$ values which range from +14.2‰ to +23.6‰ (Table 4). When present, the $H_2S$ is typically 4.0‰ to 5.6‰ lighter than the associated thiols ($n$=3) and 5.8‰ lighter than associated thiophene ($n$=2), with an exception from the $C_2h$ reservoir from well QL24 where the differences between the

**Table 3** VOSCs concentrations of the natural gas samples[a)]

| Sulfur compounds | B001-1 | | YA012-1 | | DT002-X9 | | TD61 | | W118 | | W127 | | QL24 | |
|---|---|---|---|---|---|---|---|---|---|---|---|---|---|---|
| | Con. (ppm) | Std ($\sigma$) | Con. (ppm) | Std ($\sigma$) | Con. (ppm) | Std ($\sigma$) | Con. (ppm) | Std ($\sigma$) | Con. (ppm) | Std ($\sigma$) | Con. (ppm) | Std ($\sigma$) | Con. (ppm) | Std ($\sigma$) |
| MeSH | 99.8 | – | 30 | 8 | 6.4 | – | 0.9 | – | 1.3 | – | 43.7 | – | 6.4 | – |
| EtSH | 32.5 | – | 6.1 | – | 2.6 | 0.3 | 0.5 | – | 0.9 | – | 24.9 | – | 6.4 | – |
| 2-PrSH | 1 | 0 | 0.4 | 0.2 | 0.3 | 0.1 | 0.2 | – | 0 | – | 2.3 | – | 0.6 | 0.3 |
| 1-PrSH | 0.3 | 0 | 0.9 | – | 1.3 | 0.2 | 0.1 | – | 0.2 | – | 0.5 | – | 0.7 | 0.4 |
| 2-BuSH | – | – | 0.4 | – | 0.3 | – | – | – | – | – | – | – | 0 | – |
| 1-BuSH | – | – | 0.5 | 0.3 | 1 | 0.3 | – | – | – | – | – | – | 0.1 | – |
| 1-PeSH | – | – | 0.3 | – | 0.3 | 0.1 | – | – | – | – | – | – | 0 | – |
| DMS | 1.2 | 0.2 | 0.1 | – | — | – | – | – | 0.3 | – | 4.5 | – | 0 | – |
| $CS_2$ | 0.3 | – | <0.1 | – | — | – | – | – | – | – | 0.2 | – | 0 | – |
| EMS | 0.4 | 0 | – | – | — | – | – | – | – | – | 2.1 | – | 0 | – |
| $CH_3SSH$ | 0.1 | 0 | 0.2 | – | 0.1 | 0 | – | – | – | – | – | – | 0 | – |
| DMDS | – | – | – | – | — | – | – | – | 0.2 | – | 1.6 | 0.5 | 0.1 | – |
| DEDS | – | – | – | – | — | – | – | – | – | – | 0.3 | – | 0.1 | – |
| Thiophene | – | – | 0.1 | – | 0.2 | – | – | – | – | – | – | – | — | – |

a) –, no data available; Con. is concentration

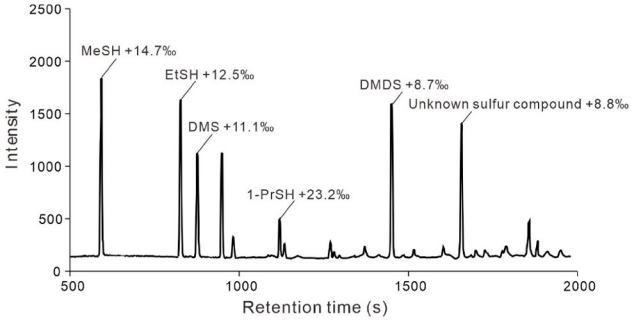


**Figure 6** Gas chromatogram of VOSCs of the W118 gas with their $\delta^{34}S$ value for individual compounds. MeSH, methanethiol; EtSH, ethanethiol; DMS, dimethylsulfide; 1-PrSH, 1-propanethiol; DMDS, dimethyl disulfide.

$H_2S$ and thiols are less than 1.7‰ (Figure 8). In contrast, the relation of $H_2S$ to the sulfides does not show a distinctive trend as it is isotopically lighter than some sulfides while being heavier than others.

## 5. Discussion

### 5.1 Identifying the origins of $H_2S$ in the Basin

The Triassic, Permian and Carboniferous reservoirs of the Sichuan Basin were the subject of plenty of previous studies that focused on gas origins, migration patterns and variable post-generation processes (Cai et al., 2003; Huang et al., 2023). The key post-generation process affecting the chemical and isotopic compositions of natural gases is interaction with $H_2S$ (Cai et al., 2003, 2013; Li et al., 2019). The $H_2S$-generating processes in petroleum reservoirs include BSR, TSR and TCA. TCA may have occurred in geological history when the available source rocks generated the gas nowadays reservoired in the Triassic, Permian and Carboniferous reservoirs. The ability of TCA to generate $H_2S$ depends exclusively on the presence of labile sulfur groups within the parent kerogen (Kutuzov et al., 2023b), and the concentrations of TCA-derived $H_2S$ depend on sulfur contents and cracking extents of source rock kerogen. Experimental investigations in closed systems have shown that TCA-derived $H_2S$ have sulfur isotopic compositions close to the parent kerogen if the associated pyrite is not decomposed (Amrani et al., 2019; Meshoulam et al., 2021). However, such an origin of $H_2S$ is rarely reported from natural reservoirs due to its low concentration and loss from reacting with iron and dissolution in formation water. An exception case was reported from Middle Triassic Leikoupo Formation in the Sichuan Basin where $H_2S$ has a $\delta^{34}S$ value of −6.0‰ (Cai et al., 2003). The $H_2S$ in the study have $\delta^{34}S$ values ranging from +14.2‰ to +23.6‰ ($n$=4), significantly heavier than all the potential source rock kerogens (Figure 7), supporting a non-TCA origin.

By contrast, the majority of natural $H_2S$ with concentrations >1% may have been generated from BSR or TSR (Orr, 1974; Cai et al., 2001). Both BSR and TSR only require the presence of organic matter, sulfate source and suitable temperatures (Orr, 1974; Elsgaard et al., 1994). Since the current reservoir temperatures (108−140°C) are too high to support bacterial activity (typically limited to <102°C; Elsgaard et al., 1994), and temperatures in the geological history were

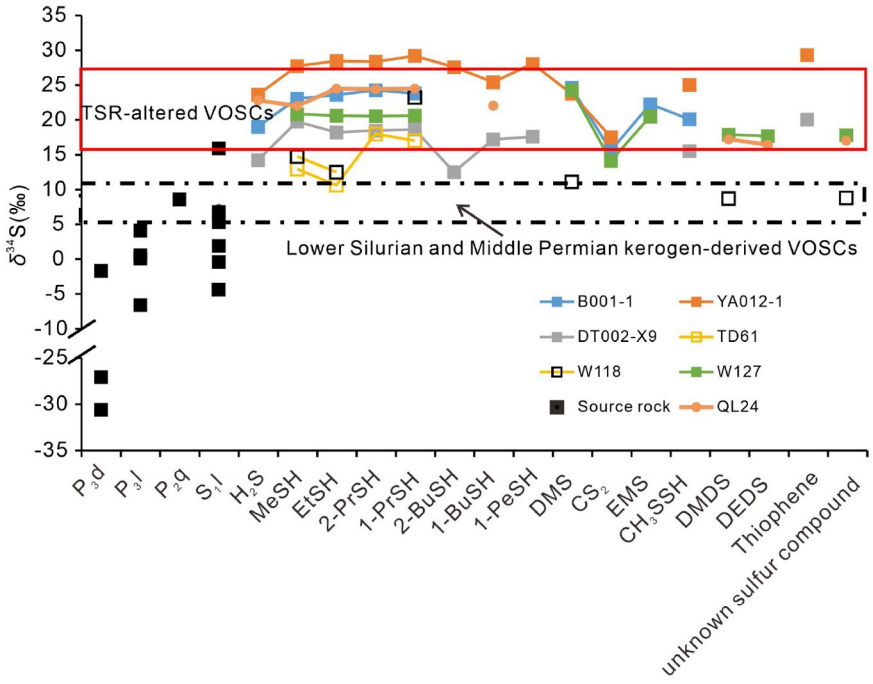


**Figure 7** Diagram showing comparison in $\delta^{34}S$ values between VOSCs from NE Sichuan Basin gases in this study and the kerogens from the potential source rocks from the Lower Silurian ($S_1l$), Middle Permian Qixia Formation ($P_2q$), Upper Permian Longtan Formation ($P_3l$) and Dalong Formation ($P_3d$). Kerogen $\delta^{34}S$ values are from Cai et al. (2010, 2017a, 2017b). MeSH, methanethiol; EtSH, ethanethiol; 2-PrSH, 2-propanethiol; 1-PrSH, 1-propanethiol; 2-BuSH, 2-butanethiol; 1-PeSH, 1-pentanethiol; DMS, dimethylsulfide; EMS, ethylmethylsulfide; DMDS, dimethyl disulfide; DEDS, diethyl disulfide.

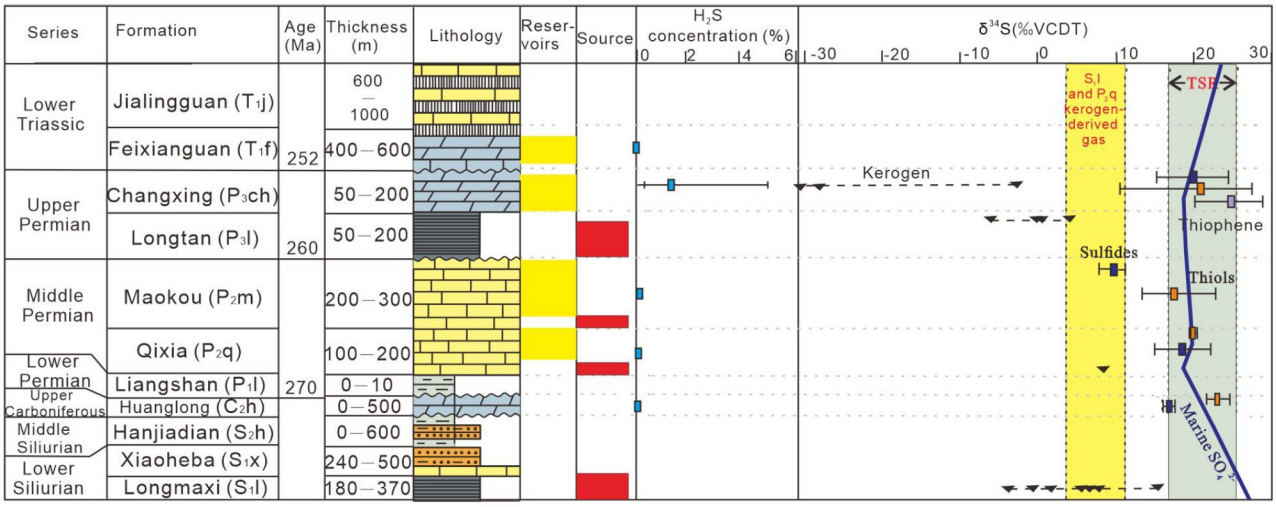


**Figure 8** Stratigraphic profile of eastern Sichuan Basin showing variation of $H_2S$ concentrations, and $\delta^{34}S$ values of kerogen, $H_2S$ and VOSCs with shaded areas for the ranges of kerogen-derived and TSR-altered VOSCs $\delta^{34}S$ values, respectively. Also plot is variation of seawater sulfate $\delta^{34}S$ value with age for comparison.

even higher (Figure 2), it is within reason to assume BSR does not take place in the studied reservoirs. Thus, the $H_2S$ is most likely to have been generated from TSR. During TSR, hydrocarbons are directly oxidized by sulfates to form $CO_2$, $H_2S$ and organic sulfur compounds as gaseous products (Krouse et al., 1988; Cai et al., 2022). As TSR reaction rates are controlled by the anhydrite dissolution, all dissolved sulfate was completely reduced to $H_2S$, thus no sulfate isotope fractionation occurs. Therefore, the $H_2S$ identified in four gases from the $C_2h$ and $P_3ch$ in the study has originated by TSR of hydrocarbons as shown by their $\delta^{34}S$ values which are close to those of seawater during the deposition of the reservoirs (Figure 9). If the source of the hydrocarbon interacting in TSR is natural gas, alkanes longer than methane are expected to be oxidized preferentially, and if the process of TSR is incomplete, only propane and ethane become $^{13}C$ enriched as their $^{12}C$-H and $^{12}C$-C will preferentially react with sulfates due to weaker bond strength during TSR, re-

**Table 4** Sulfur isotopic compositions of VOSCs and $H_2S$ of the natural gas samples[a)]

| Sulfur compounds | B001-1 | | YA012-1 | | DT002-X9 | | TD61 | | W118 | | W127 | | QL24 | |
|---|---|---|---|---|---|---|---|---|---|---|---|---|---|---|
| | $\delta^{34}$S (‰) | Std ($\sigma$) | $\delta^{34}$S (‰) | Std ($\sigma$) | $\delta^{34}$S (‰) | Std ($\sigma$) | $\delta^{34}$S (‰) | Std ($\sigma$) | $\delta^{34}$S (‰) | Std ($\sigma$) | $\delta^{34}$S (‰) | Std ($\sigma$) | $\delta^{34}$S (‰) | Std ($\sigma$) |
| MeSH | 23 | – | 27.7 | 0.4 | 19.8 | – | 12.9 | – | 16.7 | – | 20.8 | – | 22 | – |
| EtSH | 23.6 | – | 28.5 | – | 18.2 | 0.7 | 10.6 | – | 12.5 | – | 20.6 | – | 24.5 | – |
| 2-PrSH | 24.3 | 0.8 | 28.3 | 1.1 | 18.4 | 0.5 | 18 | – | – | – | 20.5 | – | 24.4 | 0.2 |
| 1-PrSH | 23.8 | 0.4 | 29.2 | – | 18.6 | 0.3 | 17 | – | 23.2 | – | 20.6 | – | 24.5 | 0.3 |
| 2-BuSH | – | – | 27.6 | – | 11.9 | – | – | – | – | – | – | – | – | – |
| 1-BuSH | – | – | 25.4 | 0.7 | 17.2 | 0.5 | – | – | – | – | – | – | 22 | – |
| 1-PeSH | – | – | 28 | – | 17.6 | 0.1 | – | – | – | – | – | – | – | – |
| DMS | 25.1 | 0.7 | 23.8 | – | – | – | – | – | 11.1 | – | 22.4 | – | – | – |
| $CS_2$ | 15.6 | – | 17.5 | – | – | – | – | – | – | – | 14.1 | – | – | – |
| EMS | 22.2 | 0.7 | – | – | – | – | – | – | – | – | 20.5 | – | – | – |
| $CH_3SSH$ | 19.5 | 0.1 | 24.3 | – | 15.5 | 0.6 | – | – | – | – | – | – | – | – |
| DMDS | – | – | – | – | – | – | – | – | 8.7 | – | 17.9 | 0.4 | 17.2 | – |
| DEDS | – | – | – | – | – | – | – | – | – | – | 17.7 | – | 16.4 | – |
| Unknown sulfur compound | – | – | – | – | – | – | – | – | 8.8 | – | 17.8 | – | 17 | – |
| Thiophene | – | – | 29.3 | – | 20 | – | – | – | – | – | – | – | – | – |
| $H_2S$ | 19 | 0.4 | 23.6 | 0.4 | 14.2 | 0.4 | – | – | – | – | – | – | 22.8 | 0.1 |

a) –, no data available

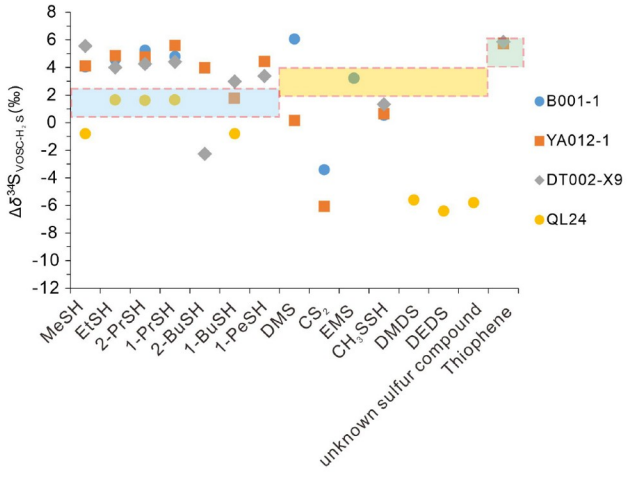


**Figure 9** Sulfur isotopic difference ($\Delta^{34}$S) between the various VOSCs of gas samples B001-1, YA012-1, DT002-X9 and QL24 with their associated $H_2S$. The shaded area represents the range of expected thermodynamic equilibrium at 160°C to 180°C for the $P_3$ch to $P_2$m and the dotted area is the range at 170°C to 190°C for the $C_2$h, the maximum temperatures the reservoirs experienced (Figure 2), based on *ab-initio* calculations presented in Amrani et al. (2019) (including uncertainty range of ±1‰). MeSH, methanethiol; EtSH, ethanethiol; 2-PrSH, 2-propanethiol; 1-PrSH, 1-propanethiol; 2-BuSH, 2-butanethiol; 1-PeSH, 1-pentanethiol; DMS, dimethylsulfide; EMS, ethylmethylsulfide; DMDS, dimethyl disulfide; DEDS, diethyl disulfide.

sulting in increase in $C_1/C_{1\text{-}5}$ ratios (Cai et al., 2003). When the majority of ethane and other heavier hydrocarbons are depleted, methane is expected to be involved in TSR and then the residual methane is expected to be enriched in both $^{13}$C and $^{2}$H (Cai et al., 2013; Liu et al., 2013; Li et al., 2019). Methane-dominated TSR in the $P_3$ch and $T_1$f reservoirs in the surrounding of the Kaijiang-Liangping trough (group 1 gases) is well indicated by the positive correlative relationships of GSI to both $C_1/C_{1\text{-}5}$ ratios and $\delta^{13}C_1$ value (Figure 3a and 3b), and between methane $\delta^{13}C_1$ and $\delta^{2}H_1$ value (Figure 4a). The group 2 gases have all GSI less than 0.8%, suggesting the gases were not or slightly altered by TSR although a $C_2$h gas from well QL24 has $H_2S$ $\delta^{34}$S value of +22.4‰, a typical product of TSR.

## 5.2 Identifying the origins of VOSCs

VOSCs including thiols can be generated by, (1) back reactions of TSR-$H_2S$ with hydrocarbons (Cai et al., 2003), which is supported by the individual compound sulfur compounds for the first time from the Ordovician Majiagou Formation reservoirs in the Ordos Basin (Kutuzov et al., 2023a), and (2) cracking of the parent source rock kerogen (Amrani et al., 2019). The W118 and TD61 gases have thiols $\delta^{34}$S values mainly from +12.5‰ to +23.2‰, which are close to those of the Permian carbonate associated sulfate (CAS) from +15.2‰ to +23.3‰ ($n$=4; Li et al., 2014). However, the associated sulfides and an unknown sulfur-bearing com-

pound from the W118 gas have much lighter values around +8.7‰, suggesting a different origin. It has been shown that the reaction of hydrocarbons with $H_2S$ to form VOSCs is inversely related to thermal stability, i.e., thiols>sulfides>thiophenes (Amrani et al., 2019). During this very early or minor TSR stage, the less stable thiols can rapidly attain sulfur isotope equilibrium with $H_2S$ (Amrani et al., 2019; Meshoulam et al., 2021). Thus, the TD61 and W118 gases may have thiols generated during TSR or sulfur isotope exchange with TSR-derived $H_2S$ while no thermally stable VOSCs are formed during this stage. This in turn resulted in the significantly heavier $\delta^{34}S$ values of thiols than other VOSCs as shown by the W118 gas. So far, it is not clear which of the VOSCs formation pathways in nature, gas-phase or liquid-phase reactions, is dominated. The liquid-phase reactions are more energetically favorable, and are widely accepted as the mechanism for methane and anhydrite reactions in gas pools despite low water saturation (Worden and Smalley, 1996; Cai et al., 2004).

When TSR is initiated, $H_2S$ is generated as a reaction product and tends to react with hydrocarbons to generate less stable thiols firstly, and the thiols can rapidly attain sulfur isotope equilibrium with $H_2S$ (Amrani et al., 2019; Meshoulam et al., 2021). Thus, the TD61 and W118 gases may have thiols generated during TSR or sulfur isotope exchange with TSR-derived $H_2S$ whilst no more thermally stable VOSCs including organic sulfides are formed during this stage. This is demonstrated by the evidence showing DMDS and an unknown sulfur compound have $\delta^{34}S$ values of about +8.7‰, being close to the source rock kerogen in the basin.

When TSR further proceeds to have GSI not more than about 1.0, more thiols and sulfides are expected to be generated from reactions of alkanes with TSR-$H_2S$ accompanied by their decomposition to short-chained compounds, and large $\delta^{34}S$ differences up to 8.1‰ exist between thiols and sulfides as shown by W127 and QL24 gases. When TSR proceeds to have GSI greater than 2.0, all VOSCs have a consistent $\delta^{34}S$ distribution as shown by DT002-X9, B001-1 and YA012-1 gases. In fact, all the TSR gases except the very minor TSR gas (W118 gas) have all thiols and sulfides $\delta^{34}S$ values mainly from +17.7‰ to +28.5‰, close to those of the CAS in the Permian and Lower Triassic reservoirs (Figures 7 and 9), suggesting that all the thiols and sulfides have been formed from hydrocarbons interactions with TSR-derived $H_2S$. The $P_3$ch and $T_1$f reservoirs have been shown to experience maximum temperatures of about 160°C to 180°C (Figure 2). At such a temperature, *Ab-initio* calculations predicted the $\Delta^{34}S_{VOSCs\text{-}H2S}$ values at isotopic equilibrium between thiols, sulfides, and thiophenes range from 1.7‰ ±1.0‰, 2.9‰±1.0‰ and 4.9‰±1.0‰, respectively (Amrani et al., 2019; Meshoulam et al., 2021), and are slightly lower for the $C_2$h reservoirs with the maximum temperatures of about 170°C to 190°C. All the thiols from an individual gas sample shows similar $\delta^{34}S$ values which are significantly higher than those in isotopic equilibrium with the associated $H_2S$ as shown by DT002-X9, B001-1 and YA012-1 gases (Table 4 and Figure 8). Similarly, relatively low $\delta^{34}S$ value of +33.5‰ has been reported to associate with ZS1C oil from Tarim Basin with extremely $^{34}S$-enriched benzothiophenes up to +40.4‰, dibenzothiophenes up to +38.5‰ and thiadiamondoids up to +41.4‰ and thiolanes up to +38.5‰ (Cai et al., 2016). All the thiophene data ($n$=2) from this study plot within the equilibrium area. These results suggest that both thiols and thiophene analyzed were formed from reaction with the TSR-derived $H_2S$. In contrast, most of the sulfides are plotted below the area (Figure 8). Different from the Alberta and Ordos Basins, the two samples with thiophene and $H_2S$ $\delta^{34}S$ values from the Sichuan Basin have thiophene in EIE with the associated $H_2S$. Unfortunately, no $H_2S$ $\delta^{34}S$ value is available to evaluate if VOSCs from W118 gas are in EIE with the $H_2S$. However, this gas has a low VOSCs concentration of 2.9 ppm, and the sulfides and the unknown sulfur-bearing compound are not in the association with $H_2S$, indicating back reactions of TSR-$H_2S$ via gas-phase formation of VOSC within the reservoir is unlikely (Kutuzov et al., 2023b) and therefore further supports gas migration, most likely, from source rocks.

### 5.3 Identifying the origins of group 1 gases

The group 1 gases in this study show wide variation in $\delta^{13}C_1$, $\delta^{2}H_{CH4}$, $\delta^{13}C_2$ and $\delta^{13}C_3$ values (Figure 4a–4c; Table 2). These parameters are related to initial gas chemical and isotopic compositions which are controlled by thermal maturity and isotopic compositions of the precursor source rock kerogen or oil, and subsequent secondary alteration in the reservoirs. An isotope-maturity model was developed by Berner and Faber (1996) and shows the $\delta^{13}C$ values of methane, ethane, and propane derived from a unique source rock are distributed along the maturity lines and towards less negative values with increasing maturity. The positive relationships between methane $\delta^{13}C_1$ and $\delta^{2}H$, $\delta^{13}C_1$ and $\delta^{13}C_2$, and $\delta^{13}C_2$ and $\delta^{13}C_3$ (Figure 4a–4c) can be explained as results from thermal cracking (TCA) alone, or mixing between gases with high and low maturity. However, the two processes are expected to result in group 1 gases plot along rather than above the $\delta^{13}C_1$ vs $\delta^{13}C_2$ line as shown in Figure 10a. Furthermore, the roughly positive correlative relationships of GSI to $\delta^{13}C_1$ (Figure 3b), well indicating that methane was oxidized during TSR. TSR shows a much larger increase in dryness and $\delta^{13}C$ values compared with TCA as demonstrated by many experiment simulations (Kiyosu and Krouse, 1989; Pan et al., 2006; Lu et al., 2012). In fact, TSR is enhanced by increasing temperature or TCA. Such an oxidation of methane results in preferential depletion of methane $^{12}C$ and $^{1}H$ (Krouse et al., 1988; Cai et al., 2003,

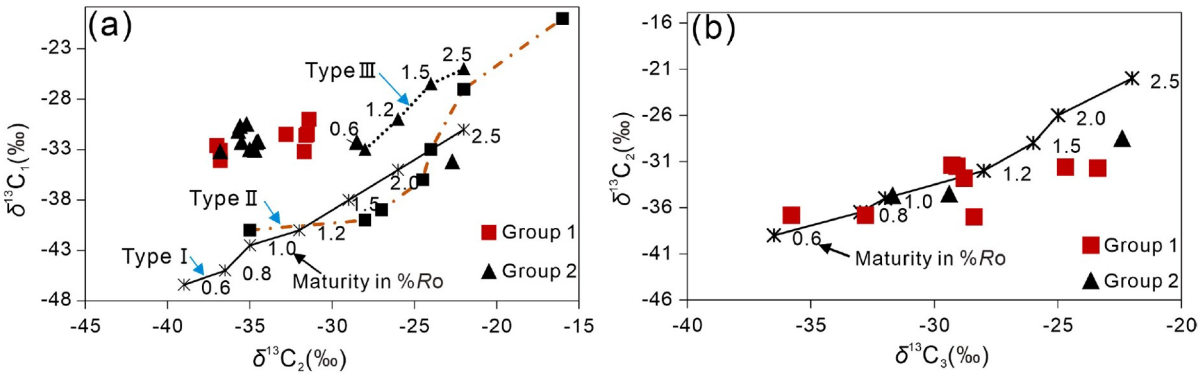


**Figure 10** Plots of $\delta^{13}C_1$ and $\delta^{13}C_2$ (a) and $\delta^{13}C_2$ and $\delta^{13}C_3$ (b), over the maturity lines for different kerogen types (I, II and III) from Berner and Faber (1996). Numbers on the line of marine organic matter indicate the maturity of the source rock in %*Ro*.

2004, 2013; Hu et al., 2014), leaving residual unreacted methane enriched in $^{13}C$ and $^{2}H$, and resulting in a positive relationship between methane $\delta^{13}C_1$ and $\delta^{2}H$ (Figure 4a). TSR has been reported to result in $\delta^{13}C_1$ values shifted to as heavy as −16.7‰ and −3‰ as reported from the Sichuan Basin and Saudi Arabia, respectively (Cai et al., 2003, 2004, 2013; Cai, 2015; Jenden et al., 2015; Wang et al., 2011). Methane in a gas is oxidized only when the dryness or $C_1/C_{1\text{-}5}$ ratio is greater than 0.97 after the depletion of $C_{2\text{-}5}$ alkanes (Cai et al., 2003, 2004). This means that $C_{2\text{-}5}$ alkanes are limited in amount and have extremely heavy $\delta^{13}C$ values when the oxidation of methane occurs (Cai et al., 2013), ruling out any possibility for the $\delta^{13}C_1>\delta^{13}C_2$ pattern to have been formed by TSR alone. The group 1 gases may have ethane and propane not significantly changed by TSR as demonstrated by evidence showing neither $\delta^{13}C_2$ nor $\delta^{13}C_3$ values of group 1 gases are related to GSI (Table 2). The gases may have $C_{2\text{-}5}$ alkanes generated from a unique source rock as supported by two aspects of evidence, (1) most of the gases have $\delta^{13}C_2$, $\delta^{13}C_3$ and $\delta^{13}C_4$ values plot along straight lines on the natural gas plot (Figure 5), and (2) the positive relationships between $\delta^{13}C_2$ and $\delta^{13}C_3$ values (Figures 4c and 10b).

From the above, it can be concluded that group 1 gases may have migrated from $P_3l$ source rock (Cai et al., 2017a, 2017b), followed by subsequent alteration in the reservoirs by TSR to different degrees with the highest GSI value for the most TSR altered gas and the lowest GSI value for least TSR gas. TD95 gas is the least TSR-altered gas with the lowest GSI value of 0.028, and may have lightest $\delta^{13}C_1\geqslant-36.8‰$ and $\delta^{13}C_2\geqslant-36.8‰$ among the group 1. YA012-1 gas is the greatest TSR-altered gas with the largest GSI value of 5.5 and shows the highest (or heaviest) $\delta^{13}C_1\geqslant-30.0‰$ among the group 1 and very low contents of ethane and other heavier alkanes. Subsequently, the group 1 gases may have mixed with non-TSR altered gases, resulting in decrease in dryness coefficient $C_1/C_{1\text{-}5}$, negative shift in $\delta^{13}C_1$ and $\delta^{13}C_2$. Thus, the TD95 gas with an apparent isotopic rollover can well be explained as the result of mixing between non TSR-altered gases with different maturity. In contrast, the YA012-1 gas must be a mixture of residual methane gas after TSR with a wetter gas, resulting in $\delta^{13}C_1>\delta^{13}C_2$.

The earlier charged pre-TSR gases from group 1 were derived from oil cracking, thus the associated solid bitumen has been used to determine the source rock of the gas. The solid bitumen shows similar biomarker and sulfur isotopic compositions to those of the $P_3l$ source rock, respectively, and thus, the $P_3l$ has been considered as the source rock of the gas (Cai et al., 2017a, 2017b). However, it is hard to determine the source rock of later charged gas. Considering that all group 1 gases have $\delta^{13}C_2$ values <−31.4‰, which is the heaviest value for the later charged gas. This value is < −28.5‰, and thus the gas must have been derived from sapropelic type organic matter (Chen et al., 2000), and thus may have been derived from further cracking of oils and bitumens in the reservoirs, or from the further cracking of the $P_3l$ source rock kerogen.

For group 1 gases, the minor-TSR TD61 gas has total VOSCs concentration of 1.7 ppm whilst intense TSR gases have total VOSCs up to 140 ppm (Table 3). However, total VOSCs concentrations do not show a correlative relationship with GSI. This is likely due to their low thermal stability. Unlike thermal stable thiodiomandoids, which show an increase with increasing TSR extents under petroleum reservoir conditions (Wei et al., 2012; Cai et al., 2016), VOSCs can be decomposed and newly generated during TSR, and thus their concentrations are not expected to increase with TSR extents, and thus cannot be used as a TSR extent proxy. Although thiophene has been shown to the only VOSC whose $\delta^{34}S$ values can correlate to the source rock (Kutuzov et al., 2023a, 2023b), as discussed above, all the VOSCs measured for sulfur isotopic compositions from group 1 may have been altered by TSR, therefore cannot be used for gas and source rock correlation purpose in the group 1.

### 5.4 Determining the source rock for the group 2 gases using VOSCs $\delta^{34}$S values

To determine the source rock for group 2 gases, which are not significantly altered by TSR, using VOSCs $\delta^{34}$S values, firstly, it is important to determine if the gases mixed with recently charged $H_2S$. If such mixing occurs, the VOSCs, especially thiols, are expected to change their $\delta^{34}$S values, thus, limiting the ability of thiols $\delta^{34}$S values to act as a proxy for gas-source rock correlation. Second, the potential source rock should not be uplifted during petroleum generation so that all sulfur compounds generated can be kept in a closed system to reach sulfur isotope equilibration (Cai et al., 2009a). For the eastern Sichuan Basin, as the potential source rocks, the Lower Silurian and Permian shales and carbonate rocks experienced progressive burial during oil and gas generation without being significantly uplifted during the Permian to the Jurassic period (Figure 2), and there was no recent migration of natural gas (Huang et al., 2023), thus no $H_2S$ is expected to be added to the reservoirs and alter the VOSCs and oil $\delta^{34}$S values, thus, there exist no more than 2‰ to 5‰ differences in sulfur isotopic composition between source rock and oil or VOSCs based on experimental simulations under closed systems and case studies (Orr, 1986; Idiz et al., 1990; Amrani et al., 2005, 2019; Cai et al., 2009a, 2015; Rosenberg et al., 2017; Greenwood et al., 2018). Other post-generation processes of sulfur compounds, such as diffusion and dissolution to influence sulfur isotopic compositions have to be considered. However, it is not clear if diffusion can change VOSCs $\delta^{34}$S values. Considering that VOSCs have very low solubilities in the water phase and small mass difference even for the smallest compounds between $CH_3{}^{32}SH$ and $CH_3{}^{34}SH$, and the differences will be smaller if the molecules contain more carbon, the fractionation due to diffusion is expected to be small unless the migration distance is up to thousand kilometers. Based on the same reason, gas dissolution from an oil may have small sulfur isotope fractionation. Further work should be done to verify it.

On the other hand, the W118 gas produced from the $P_2$m reservoirs has a very low GSI of 0.009, suggesting no alteration by TSR. This gas has thiols $\delta^{34}$S values from +12.5‰ to +23.2‰, close to or higher than the Permian seawater sulfate (+15.2‰ to +23.3‰, $n$=4; Li et al., 2014), suggesting that at least part of the less stable thiols may have been generated or sulfur isotope exchanged with TSR-$H_2S$, adopt $\delta^{34}$S values of the $H_2S$ and its parent sulfate, and thus, their $\delta^{34}$S values cannot be used for the gas-source rock correlation. In contrast, DMDS and an unknown sulfur-bearing compound are more thermally stable, and may have been mainly derived from the source rock kerogen cracking in this case with very minor TSR extents. This proposal is supported by the similarity in $\delta^{34}$S values of these compounds to those of the source rock kerogens: the two compounds show $\delta^{34}$S values of +8.7‰ and +8.8‰, which are close to those of the $S_1$l source rock from −4.4‰ to +15.9‰ with an average of +4.6‰ ($n$=7; Cai et al., 2017a, 2017b), and a $P_2$q source rock with the value of +8.7‰ (Cai et al., 2010), but significantly higher than those of the $P_3$l from −6.6‰ to +4.1‰ with an average of −0.5‰ ($n$=4), and the $P_3$d from −30.6‰ to +5.5‰ with an average of −13.5‰ ($n$=4) (Cai et al., 2017a, 2017b; Figure 7). Assuming the sulfides preserve the $\delta^{34}$S of the kerogen which generated them, the observed sulfides are likely to have been derived from the $S_1$l and/or $P_2$q source rocks, both showing similar kerogen $\delta^{34}$S values (Figures 7 and 9) but different maturities.

Seismic cross section shows that faults developed during both the Permian and Jurassic cut through the Lower Silurian (Figure 11), providing pathways for the gas to have migrated upwards from the Lower Silurian to the Permian and Lower

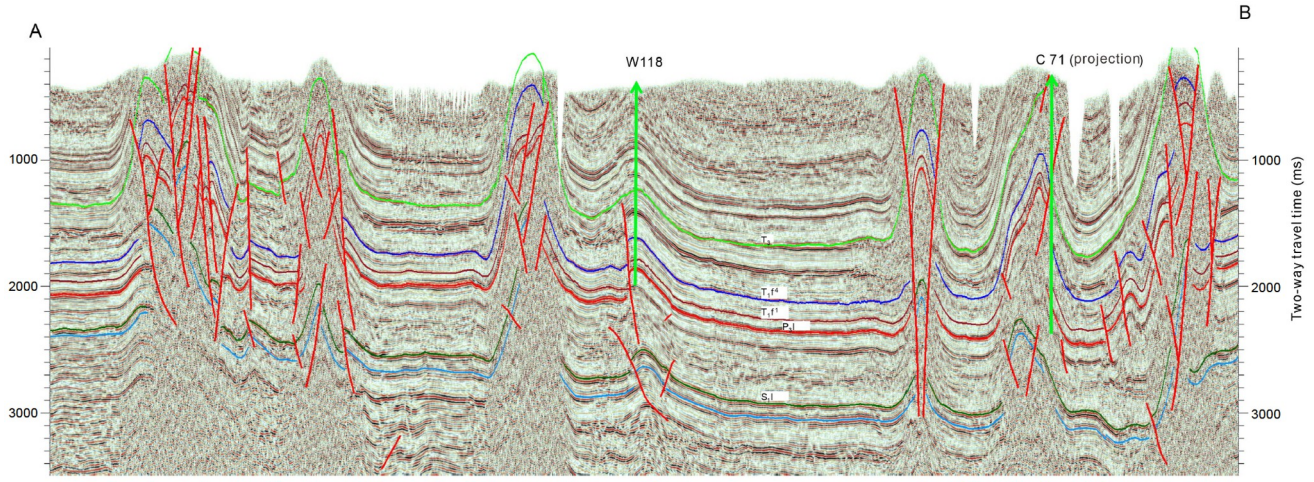


**Figure 11** Cross seismic section AB in the south to the Kaijiang-Liangping Trough showing faults cut through Lower Silurian and Permian source rocks, providing fluid conduit for petroleum to up-migrate to the Permian and Lower Triassic reservoirs. See AB location in Figure 1a.

Triassic in the eastern Sichuan Basin. The Lower Silurian and Middle Permian source rocks show a significant difference in maturity during the main hydrocarbon generation in the period from Late Triassic to Jurassic period (Wang et al., 2013; Huang et al., 2023), thus the QL22 gas presumedly derived from a high maturity Lower Silurian source rock shows $C_1/C_{1\text{-}5}$ of 0.998, $\delta^{13}C_1$ of −30.7‰ and $\delta^2H$ of −123.6‰, and the non-TSR W061-1 gas presumedly derived from a low maturity Middle Permian source rock shows $C_1/C_{1\text{-}5}$ of 0.948, and methane $\delta^{13}C_1$ of −34.2‰ and $\delta^2H$ of −134‰. The mixing of the two endmember gases may have resulted in the positive correlative relationships between methane $\delta^{13}C_1$ and $\delta^2H$ (Figure 4a), between methane $\delta^{13}C_2$ and $\delta^{13}C_3$ (Figure 4c), and the range of $C_1/C_{1\text{-}5}$ ratios between 0.948 and 0.998 (Table 1). Such mixing may have resulted in the group 2 gases with $\delta^{13}C_1>\delta^{13}C_2$.

The proposal for the gases source rocks is supported by the following lines of evidence: (1) the $P_3$l oil-prone source rocks are found to distribute in the Bazhong-Dazhou depression within the Kaijiang-liangping trough (Figure 1), and thus it is unlikely to have contributed gas to the $P_3$ch-$T_1$f gases in the south to the Kaijiang-liangping area. (2) All the group 2 gases except an anomaly from well W061-1 have $\delta^{13}C_2$ values lighter than −28.5‰, a typical feature for an oil-prone kerogen-derived gas (Chen et al., 2000). Both the $S_1$l and $P_2$m source rocks were deposited under a marine environment and show sapropelic-type organic matter (Huang et al., 2023). (3) The $S_1$l source rocks are distributed in the entire eastern Sichuan Basin whilst the $P_2$m source rock shows the much higher gas generation intensity near well W127 area (~$60\times10^8$ $m^3/km^2$) in the south to the Kaijiang-Liangping area than near Well YA001 (< ~$10\times10^8$ $m^3/km^2$) in the north (Huang et al., 2016), providing the evidence for more gases to have generated from the $S_1$l and $P_2$m source rocks and then accumulated in the southern $C_2$h to $T_1$f reservoirs. This conclusion is supported by molecular and carbon isotopic compositions and gas charge history rebuilding (Wang et al., 2013; Hu D F et al., 2020; Huang et al., 2023).

## 6. Conclusion

The gases in the study are divided into two groups. The group 1 gases from the $P_3$ch-$T_1$f reservoirs from the surrounding of the Kaijiang-liangping trough may have been derived from source rocks different from the group 2 gases from the $P_3$ch-$T_1$f reservoirs in the south and from $C_2$h to $P_2$m reservoirs in the eastern Sichuan Basin. The group 1 gases may have been derived from the $P_3$l source rock and experienced methane-dominated TSR, resulting in heavier methane $\delta^{13}C_1$ and $\delta^2H$ values and all VOSCs approaching sulfur isotope equilibrium with $H_2S$ produced from TSR. Subsequently, the gases mixed with small amount of later charged relatively $^{13}C$-depleted gas, and thus show abnormally light $\delta^{13}C_2$ values. The group 2 gases may have not significantly altered by TSR, and have been derived from the Lower Silurian and Middle Permian source rocks, and thus have $\delta^{34}S$ values of relatively stable VOSCs, including sulfides and an unknown sulfur-bearing compound, close to those of the source rocks kerogens. It is very likely for the mixing of the gases from the two different maturity source rocks to have led to the group 2 gases showing carbon isotope reversal, or $\delta^{13}C_1>\delta^{13}C_2$. This case study shows that the combination of VOSCs sulfur isotopic compositions with chemical and $^{13}C$, $^2H$ isotopic compositions of $C_1$–$C_5$ of natural gas can be used as a direct method to determine its source rock, mixing and secondary alteration, especially TSR. This method in combination with seismic data can be used to make decision on favorable targets for methane-dominated gas pools.

**Acknowledgements** *Thanks should be given to the two reviewers for their constructive comments which help to improve the earlier manuscript. This study was financially supported by the National Natural Science Foundation of China (Grant No. 41961144023) and the Israeli Science Foundation (Grant No. 3195/19).*

**Conflict of interest** The authors declare that they have no conflict of interest.

## References

Amrani A. 2014. Organosulfur compounds: Molecular and isotopic evolution from biota to oil and gas. Annu Rev Earth Planet Sci, 42: 733–768

Amrani A, Lewan M D, Aizenshtat Z. 2005. Stable sulfur isotope partitioning during simulated petroleum formation as determined by hydrous pyrolysis of Ghareb Limestone, Israel. Geochim Cosmochim Acta, 69: 5317–5331

Amrani A, Zhang T, Ma Q, Ellis G S, Tang Y. 2008. The role of labile sulfur compounds in thermochemical sulfate reduction. Geochim Cosmochim Acta, 72: 2960–2972

Amrani A, Sessions A L, Adkins J F. 2009. Compound-specific $\delta^{34}S$ analysis of volatile organics by coupled GC/multicollector-ICPMS. Anal Chem, 81: 9027–9034

Amrani A, Rosenberg Y O, Meshoulam A, Said-Ahmad W, Turich C, Luu N, Jacksier T, Stankiewicz A, Feinstein S, Shurki A. 2019. Sulfur isotopic composition of gas-phase organic sulfur compounds provides insights into the thermal maturation of organic-rich rocks. Geochim Cosmochim Acta, 259: 91–108

Behar F, Kressmann S, Rudkiewicz J L, Vandenbroucke M. 1991. Experimental simulation in a confined system and kinetic modelling of kerogen and oil cracking. Org Geochem, 19: 173–189

Berner U, Faber E. 1996. Empirical carbon isotope/maturity relationships for gases from algal kerogens and terrigenous organic matter, based on dry, open-system pyrolysis. Org Geochem, 24: 947–955

Bildstein O, Worden R H, Brosse E. 2001. Assessment of anhydrite dissolution as the rate-limiting step during thermochemical sulfate reduction. Chem Geol, 176: 173–189

Cai C F. 2015. Origin of the C, $P_3$-$T_1$ gases in the northern Sichuan Basin: Constraints from gas and solid bitumen geochemistry. Chengdu: 5th International Meeting of Natural Gas Geochemistry

Cai C F, Hu W S, Worden R H. 2001. Thermochemical sulphate reduction

in Cambro-Ordovician carbonates in Central Tarim. Mar Pet Geol, 18: 729–741
Cai C F, Worden R H, Bottrell S H, Wang L S, Yang C. 2003. Thermochemical sulphate reduction and the generation of hydrogen sulphide and thiols (mercaptans) in Triassic carbonate reservoirs from the Sichuan Basin, China. Chem Geol, 202: 39–57
Cai C F, Xie Z Y, Worden R H, Hu G Y, Wang L S, He H. 2004. Methane-dominated thermochemical sulphate reduction in the Triassic Feixianguan Formation east Sichuan Basin, China: Towards prediction of fatal $H_2S$ concentrations. Mar Pet Geol, 21: 1265–1279
Cai C F, Hu G Y, He H, Li J, Li J F, Wu Y S. 2005. Geochemical characteristics and origin of natural gas and thermochemical sulphate reduction in Ordovician carbonates in the Ordos Basin, China. J Pet Sci Eng, 48: 209–226
Cai C F, Li K K, Ma A L, Zhang C M, Xu Z M, Worden R H, Wu G H, Zhang B S, Chen L X. 2009a. Distinguishing Cambrian from Upper Ordovician source rocks: Evidence from sulfur isotopes and biomarkers in the Tarim Basin. Org Geochem, 40: 755–768
Cai C F, Zhang C M, Cai L L, Wu G H, Jiang L, Xu Z M, Li K K, Ma A L, Chen L X. 2009b. Origins of Palaeozoic oils in the Tarim Basin: Evidence from sulfur isotopes and biomarkers. Chem Geol, 268: 197–210
Cai C F, Li K, Zhu Y, Xiang L, Jiang L, Tenger L, Cai X, Cai L L. 2010. TSR origin of sulfur in Permian and Triassic reservoir bitumen, East Sichuan Basin, China. Org Geochem, 41: 871–878
Cai C F, Zhang C, He H, Tang Y. 2013. Carbon isotope fractionation during methane-dominated TSR in East Sichuan Basin gasfields, China: A review. Mar Pet Geol, 48: 100–110
Cai C F, Zhang C M, Worden R H, Wang T K, Li H X, Jiang L, Huang S Y, Zhang B S. 2015. Application of sulfur and carbon isotopes to oil-source rock correlation: A case study from the Tazhong area, Tarim Basin, China. Org Geochem, 83-84: 140–152
Cai C F, Amrani A, Worden R H, Xiao Q, Wang T, Gvirtzman Z, Li H, Said-Ahmad W, Jia L. 2016. Sulfur isotopic compositions of individual organosulfur compounds and their genetic links in the Lower Paleozoic petroleum pools of the Tarim Basin, NW China. Geochim Cosmochim Acta, 182: 88–108
Cai C F, Xiang L, Yuan Y, Xu C, He W, Tang Y, Borjigin T. 2017a. Sulfur and carbon isotopic compositions of the Permian to Triassic TSR and non-TSR altered solid bitumen and its parent source rock in NE Sichuan Basin. Org Geochem, 105: 1–12
Cai C F, Xu C L, He W X, Zhang C M, Li H X. 2017b. Biomarkers and C and S Isotopes of the Permian to Triassic solid bitumen and its potential source rocks in NE Sichuan Basin. Geofluids, 2017: 1–14
Cai C F, Li H, Li K K, Wang D. 2022. Thermochemical sulfate reduction in sedimentary basins and beyond: A review. Chem Geol, 607: 121018
Cao C H, Lv Z G, Li L W, Du L. 2016. Geochemical characteristics and implications of shale gas from the Longmaxi Formation, Sichuan Basin, China. J Nat Gas Geosci, 1: 131–138
Chen J F, Xu Y C, Huang D F. 2000. Geochemical characteristics and origin of natural gas in Tarim basin, China. AAPG Bull, 84: 591–606
Chung H M, Gormly J R, Squires R M. 1988. Origin of gaseous hydrocarbons in subsurface environments: Theoretical considerations of carbon isotope distribution. Chem Geol, 71: 97–104
Claypool G E, Holser W T, Kaplan I R, Sakai H, Zak I. 1980. The age curves of sulfur and oxygen isotopes in marine sulfate and their mutual interpretation. Chem Geol, 28: 199–260
Elsgaard L, Isaksen M F, Jørgensen B B, Alayse A M, Jannasch H W. 1994. Microbial sulfate reduction in deep-sea sediments at the Guaymas Basin hydrothermal vent area: Influence of temperature and substrates. Geochim Cosmochim Acta, 58: 3335–3343
Galimov E M. 1988. Sources and mechanisms of formation of gaseous hydrocarbons in sedimentary rocks. Chem Geol, 71: 77–95
Giesemann A, Jaeger H J, Norman A L, Krouse H R, Brand W A. 1994. Online sulfur-isotope determination using an elemental analyzer coupled to a mass spectrometer. Anal Chem, 66: 2816–2819
Greenwood P F, Mohammed L, Grice K, McCulloch M, Schwark L. 2018. The application of compound-specific sulfur isotopes to the oil-source rock correlation of Kurdistan petroleum. Org Geochem, 117: 22–30
Gvirtzman Z, Said-Ahmad W, Ellis G S, Hill R J, Moldowan J M, Wei Z, Amrani A. 2015. Compound-specific sulfur isotope analysis of thiadiamondoids of oils from the Smackover Formation, USA. Geochim Cosmochim Acta, 167: 144–161
He D, Li D, Zhang G. 2011. Fromation and evolution of muticycle superposed Sichuan Basin. Chin J Geol, 46: 589–606
Hu D F, Wang L J, Zhang H R, Duan J B, Xia W Q, Liu Z J, Wei Q C, Pan L. 2020. Discovery of carbonate source rock gas reservoir and its petroleum geological implications: A case study of the gas reservoir in the first Member of Middle Permian Maokou Formation in the Fuling area, Sichuan Basin (in Chinese). Nat Gas Indu B, 40: 23–33
Hu G Y, Yu C, Gong D Y, Tian X W, Wu W. 2014. The origin of natural gas and influence on hydrogen isotope of methane by TSR in the Upper Permian Changxing and the Lower Triassic Feixianguan Formations in northern Sichuan Basin, SW China. Energy Explor Exploitation, 32: 139–158
Hu Y J, Cai C F, Pederson C L, Liu D W, Jiang L, He X Y, Immenhauser A. 2020. Dolomitization history and porosity evolution of a giant, deeply buried Ediacaran gas field (Sichuan Basin, China). Precambrian Res, 338: 105595
Huang S P, Jiang Q, Wang Z C, Su W, Feng Q F, Feng Z Q. 2016. Differences between the Middle Permian Qixia and Maokou source rocks in the Sichuan Basin (in Chinese). Nat Gas Indu, 36: 26–34
Huang S P, Jiang Q, Jiang H, Tang Q, Zeng F, Lu W, Hao C, Yuan M, Wu Y. 2023. Genetic and source differences of gases in the Middle Permian Qixia and Maokou formations in the Sichuan Basin, SW China. Org Geochem, 178: 104574
Idiz E F, Tannenbaum E, Kaplan I R. 1990. Pyrolysis of high-sulfur Monterey kerogens—Stable isotope of sulfur, carbon and hydrogen. In: Orr W L, White C M, eds. Geochemistry of Sulfur in Fossil Fuels. Symposium Series 429. American Chemical Society. 575–591
James A T. 1983. Correlation of natural gas by use of carbon isotopic distribution between hydrocarbon components. AAPG Bull, 67: 1176–1191
Jenden P D, Titley P A, Worden R H. 2015. Enrichment of nitrogen and $^{13}C$ of methane in natural gases from the Khuff Formation, Saudi Arabia, caused by thermochemical sulfate reduction. Org Geochem, 82: 54–68
Kiyosu Y, Krouse H R. 1989. Carbon isotope effect during abiogenic oxidation of methane. Earth Planet Sci Lett, 95: 302–306
Krouse H R, Viau C A, Eliuk L S, Ueda A, Halas S. 1988. Chemical and isotopic evidence of thermochemical sulphate reduction by light hydrocarbon gases in deep carbonate reservoirs. Nature, 333: 415–419
Kutuzov I, Said-Ahmad W, Turich C, Jiang C, Luu N, Jacksier T, Amrani A. 2021. The molecular and sulfur isotope distribution of volatile compounds in natural gases and condensates from Alberta, Canada. Org Geochem, 151: 104129
Kutuzov I, Wang D, Cai C F, Amrani A. 2023a. Tracking the origin of Ordovician natural gas in the Ordos basin using volatile sulfur compounds. Mar Pet Geol, 157: 106488
Kutuzov I, Xiao Q L, Cai C F, Amrani A. 2023b. Formation of volatile organic sulfur compounds by low thermal maturation of source rocks: A geochemical proxy for natural gas. Mar Pet Geol, 158: 106531
Li K K, Cai C F, Hou D J, He X Y, Jiang L, Jia L Q, Cai L L. 2014. Origin of high $H_2S$ concentrations in the Upper Permian Changxing reservoirs of the Northeast Sichuan Basin, China. Mar Pet Geol, 57: 233–243
Li K K, George S C, Cai C F, Gong S, Sestak S, Armand S, Zhang X F. 2019. Fluid inclusion and stable isotopic studies of thermochemical sulfate reduction: Upper Permian and Lower Triassic gasfields, northeast Sichuan Basin, China. Geochim Cosmochim Acta, 246: 86–108
Li Y J, Xu F B, Zeng L Y, Zhang W, Li M L, Liao Y S, Chen W D. 2021. Gas source in Lower Permian Maokou Formation and gas accumulation in the syncline area of eastern Sichuan basin. J Pet Sci Eng, 206: 109044
Liu D W, Cai C F, Hu Y J, Peng Y Y, Jiang L. 2021. Multistage dolomitization and formation of ultra-deep Lower Cambrian Longwangmiao Formation reservoir in central Sichuan Basin, China. Mar Pet Geol,

123: 104752
Liu Q Y, Worden R H, Jin Z J, Liu W H, Li J, Gao B, Zhang D W, Hu A P, Yang C. 2013. TSR versus non-TSR processes and their impact on gas geochemistry and carbon stable isotopes in Carboniferous, Permian and Lower Triassic marine carbonate gas reservoirs in the Eastern Sichuan Basin, China. Geochim Cosmochim Acta, 100: 96–115
Lu H, Greenwood P, Chen T, Liu J, Peng P. 2012. The separate production of $H_2S$ from the thermal reaction of hydrocarbons with magnesium sulfate and sulfur: Implications for thermal sulfate reduction. Appl Geochem, 27: 96–105
Machel H G, Krouse H R, Sassen R. 1995. Products and distinguishing criteria of bacterial and thermochemical sulfate reduction. Appl Geochem, 10: 373–389
Meshoulam A, Amrani A. 2017. Sulfur isotope exchange between thiophenes and inorganic sulfur compounds under hydrous pyrolysis conditions. Org Geochem, 103: 79–87
Meshoulam A, Ellis G S, Said Ahmad W, Deev A, Sessions A L, Tang Y C, Adkins J F, Liu J Z, Gilhooly W P, Aizenshtat Z, Amrani A. 2016. Study of thermochemical sulfate reduction mechanism using compound specific sulfur isotope analysis. Geochim Cosmochim Acta, 188: 73–92
Meshoulam A, Said-Ahmad W, Turich C, Luu N, Jacksier T, Shurki A, Amrani A. 2021. Experimental and theoretical study on the formation of volatile sulfur compounds under gas reservoir conditions. Org Geochem, 152: 104175
Orr W L. 1974. Changes in sulfur content and isotopic-ratios of sulfur during petroleum maturation—Study of Big Horn Basin paleozoic oils. AAPG Bull, 58: 2295–2318
Orr W L. 1986. Kerogen/asphaltene/sulfur relationships in sulfur-rich Monterey oils. Org Geochem, 10: 499–516
Pan C C, Yu L P, Liu J Z. 2006. Chemical and carbon isotopic fractionations of gaseous hydrocarbons during abiogenic oxidation. Earth Planet Sci Lett, 246: 70–89
Prinzhofer A, Mello M R, Takaki T. 2000. Geochemical characterization of natural gas: A physical multivariable approach and its applications in maturity and migration estimates. AAPG Bull, 84: 1152–1172
Reber S D, Cordes G T. 1995. Modifications to the Finnigan MAT 271 mass spectrometer in the Inorganic Gas Analysis Lab (No. SAND-95-0961). Sandia National Lab(SNL-NM), Albuquerque, NM (United States), doi: 10.2172/106522
Rosenberg Y O, Meshoulam A, Said-Ahmad W, Shawar L, Dror G, Reznik I J, Feinstein S, Amrani A. 2017. Study of thermal maturation processes of sulfur-rich source rock using compound specific sulfur isotope analysis. Org Geochem, 112: 59–74
Said-Ahmad W, Wong K, Mcnall M, Shawar L, Jacksier T, Turich C, Stankiewicz A, Amrani A. 2017. Compound-specific sulfur isotope analysis of petroleum gases. Anal Chem, 89: 3199–3207
Schoell M. 1980. The hydrogen and carbon isotopic composition of methane from natural gases of various origins. Geochim Cosmochim Acta, 44: 649–661
Shawar L, Said-Ahmad W, Ellis G S, Amrani A. 2020. Sulfur isotope composition of individual compounds in immature organic-rich rocks and possible geochemical implications. Geochim Cosmochim Acta, 274: 20–44
Souza I V A F, Ellis G S, Ferreira A A, Guzzo J V P, Díaz R A, Albuquerque A L S, Amrani A. 2022. Geochemical characterization of natural gases in the pre-salt section of the Santos Basin (Brazil) focused on hydrocarbons and volatile organic sulfur compounds. Mar Pet Geol, 144: 105763
Wang W C, Zhang X B, Luo H Y, Li L W. 2011. Carbon isotopic characteristics of hydrocarbons and $CO_2$ if $H_2S$-rich natural gases and their origin in Northeastern Sichuan Basin (in Chinese). Nat Gas Geosci, 22: 136–143
Wang Y P, Zhao C Y, Wang H J, Wang Z Y, Wang Z C. 2013. Origins of natural gases from marine strata in Northeastern Sichuan Basin (China) from carbon molecular moieties and isotopic data. J Asian Earth Sci, 65: 13–20
Wang Z C, Jiang Q C, Huang S P, Zhou H, Feng Q F, Dai X F, Lu W H, Ren M Y. 2018. Geological conditions for massive accumulation of natural gas in the Mid-Permian Maokou Fm of the Sichuan Basin (in Chinese). Nat Gas Ind, 38: 30–38
Wei Z B, Walters C C, Moldowan J M, Mankiewicz P J, Pottorf R J, Xiao Y T, Maze W, Nguyen P T H, Madincea M E, Phan N T, Peters K E. 2012. Thiadiamondoids as proxies for the extent of thermochemical sulfate reduction. Org Geochem, 44: 53–70
Whiticar J M. 1994. Correlation of natural gases with their sources. In: Magoon B L, Dow G W, eds. The Petroleum System from Source to Trap, 60. AAPG Memoir. 261–283
Worden R H, Smalley P C. 1996. $H_2S$-producing reactions in deep carbonate gas reservoirs: Khuff Formation, Abu Dhabi. Chem Geol, 133: 157–171
Xiao Q, Cai S, Liu J. 2021. Microbial and thermogenic hydrogen sulfide in the Qianjiang Depression of Jianghan Basin: Insights from sulfur isotope and volatile organic sulfur compounds measurements. Appl Geochem, 126: 104865

(Editorial handling: Quanyou LIU)